

The Evidence Lower Bound of Variational Autoencoders Converges to a Sum of Three Entropies

Jörg Lücke¹, Dennis Forster¹, Zhenwen Dai²
 joerg.luecke@uol.de, dennis.forster@uol.de, zhenwend@spotify.com

¹ Machine Learning Lab, University of Oldenburg, Germany

² Spotify, London, UK

Abstract

The central objective function of a variational autoencoder (VAE) is its variational lower bound. Here we show that for standard VAEs the variational bound converges to a value given by the sum of three entropies: the (negative) entropy of the latent distribution, the expected (negative) entropy of the observable distribution, and the average entropy of the variational distributions. Our derived analytical results are exact and apply for small as well as complex neural networks for decoder and encoder. Furthermore, they apply for finitely and infinitely many data points and at any stationary point (including local and global maxima). As a consequence, we show that the variance parameters of encoder and decoder play the key role in determining the values of variational bounds at stationary points. Furthermore, the obtained results can allow for closed-form analytical expressions at points of convergence, which may be unexpected as neither variational lower bounds of VAEs nor log-likelihoods of VAEs are closed-form during learning. As our main contribution, we provide the proofs for convergence of standard VAEs to sums of entropies. Furthermore, we numerically verify our analytical results and discuss some potential applications. The obtained equality to entropy sums provides novel information on those points in parameter space that variational learning converges to. As such, we believe, they can contribute to our understanding of established as well as novel VAE approaches.

1 Introduction

Variational autoencoders (VAEs; e.g. Kingma and Welling, 2014; Rezende et al., 2014) have emerged as very popular models for unsupervised learning. They combine elements of probabilistic generative models and deep neural networks (DNNs). Generative models describe a given data distribution using parametrized probability density functions. A standard VAE is a model with one set of latent variables and one set of observable variables, where the two sets are coupled by deep neural networks (DNNs) for encoder and decoder. Let us denote the vector of latent variables by $\vec{z} \in \mathbb{R}^H$ and the vector of observed variables by $\vec{x} \in \mathbb{R}^D$. The decoder of a standard VAE is then given by:

Model VAE-1

$$p_{\Theta}(\vec{z}) = \mathcal{N}(\vec{z}; \vec{0}, \mathbb{1}), \quad p_{\Theta}(\vec{x} | \vec{z}) = \mathcal{N}(\vec{x}; \vec{\mu}_{\Theta}(\vec{z}), \sigma^2 \mathbb{1}) \quad \text{with} \quad \vec{\mu}_{\Theta}(\vec{z}) = \text{DNN}_{\mu}(\vec{z}; W), \quad (1)$$

where $\vec{\mu}_{\Theta}$ is a non-linear function parametrized by a DNN with parameters W (we take W to include all weight matrices and biases). $p_{\Theta}(\vec{z})$ denotes the prior distribution, and $p_{\Theta}(\vec{x} | \vec{z})$ is the observable distribution (both are Gaussian). We denote by $\Theta = (W, \sigma^2)$ the set of all parameters for the decoder.

The encoder of a standard VAE is (for a data point $\vec{x}^{(n)}$) defined by the following distribution:

$$q_{\Phi}^{(n)}(\vec{z}) = \mathcal{N}(\vec{z}; \vec{\nu}_{\Phi}(\vec{x}^{(n)}), \mathcal{T}_{\Phi}(\vec{x}^{(n)})), \quad \mathcal{T}_{\Phi}(\vec{x}^{(n)}) = \begin{pmatrix} \tau_1^2(\vec{x}^{(n)}; \Phi) & & \\ & \ddots & \\ & & \tau_H^2(\vec{x}^{(n)}; \Phi) \end{pmatrix}, \quad (2)$$

where $\mathcal{T}_\Phi(\vec{x}^{(n)})$ is a diagonal covariance matrix with H positive entries $\tau_h^2(\vec{x}^{(n)}; \Phi)$ on the diagonal. The vectorial non-linearity $\vec{\tau}_\Phi^2(\vec{x}) = (\tau_1^2(\vec{x}; \Phi), \dots, \tau_H^2(\vec{x}; \Phi))^T$ for the covariance and the non-linearity $\vec{\nu}_\Phi(\vec{x})$ for the mean are both given by DNNs:

$$\vec{\nu}_\Phi(\vec{x}) = \text{DNN}_\nu(\vec{x}; V), \quad \vec{\tau}_\Phi^2(\vec{x}) = \text{DNN}_\tau(\vec{x}; T), \quad (3)$$

where V and T both include all weights and biases of their DNN, respectively (the subscripts are used to distinguish the DNNs). We denote by $\Phi = (V, T)$ the set of all encoder parameters.

Given a set of N data points $\vec{x}^{(n)}$, standard VAE learning algorithms seek decoder and encoder parameters (i.e., Θ and Φ) that maximize the central learning objective of VAEs: the variational lower bound. Two common (and mathematically equivalent) forms of the lower bound are:

$$\mathcal{F}(\Phi, \Theta) = \frac{1}{N} \sum_n \int q_\Phi^{(n)}(\vec{z}) \log(p_\Theta(\vec{x}^{(n)} | \vec{z}) p_\Theta(\vec{z})) d\vec{z} - \frac{1}{N} \sum_n \int q_\Phi^{(n)}(\vec{z}) \log(q_\Phi^{(n)}(\vec{z})) d\vec{z} \quad (4)$$

$$= \frac{1}{N} \sum_n \int q_\Phi^{(n)}(\vec{z}) \log(p_\Theta(\vec{x}^{(n)} | \vec{z})) d\vec{z} - \frac{1}{N} \sum_n D_{\text{KL}}(q_\Phi^{(n)}(\vec{z}), p_\Theta(\vec{z})), \quad (5)$$

where $D_{\text{KL}}(q(\vec{z}), p(\vec{z}))$ denotes the Kullback-Leibler divergence between two distributions.

The variational lower bound is for all encoder parameters Φ smaller or equal to the log-likelihood $\mathcal{L}(\Theta) = \sum_n \log(p_\Theta(\vec{x}^{(n)}))$ which is defined by the decoder. As a tribute to its importance, the variational lower bound is known under different names, including *evidence lower bound* (ELBO; e.g. Blei et al., 2017) or *variational free energy* (e.g. Neal and Hinton, 1998). Variational bounds, which are defined through their *variational distributions* $q_\Phi^{(n)}(\vec{z})$, can usually be optimized more efficiently than the likelihood itself. However, the variational bound is (like the likelihood) usually not analytically tractable for VAEs (and for many other models). The intractability of the bound for VAEs stems from the first summand (in Eqn.4 or Eqn.5): Because of (potentially very intricate) DNN non-linearities of standard VAEs, the integrals can not be solved analytically. The central research challenge for training VAEs is therefore the development of efficient methods to approximate intractable integrals of variational bounds. Indeed, the suggestion of efficient methods to estimate gradients of Eqn.(5) using sampling and reparametrization (Kingma and Welling, 2014; Rezende et al., 2014) has played the key role in the establishment of the field of VAE research.

Because of the potentially complex DNNs of VAEs few exact theoretical results may be expected especially in realistic settings, i.e., for real and finite data sets and convergence to local optima. Therefore, maybe surprisingly, we here provide an exact result for all standard VAEs: we show that the variational bound is at convergence given by a sum of the entropies of their constituting distributions.

The derived results are based on exploiting properties of the variational bound (5) at stationary points, i.e., to those points in parameter space where the variational bound reaches an extremum (local optima, saddle points and global optima). Throughout the paper, we refer with ‘at convergence’ to such stationary points but we remark that VAE parameters will in practice only reach the vicinity of stationary points (due to finite learning times and stochasticity; we elaborate in Appendix D).

For VAE-1, the final result is sufficiently concise to be stated here initially (before we discuss its derivation, related work, and more general VAEs later on). The result states that at all stationary points of the variational lower bound (5) of VAE-1 it applies:

$$\mathcal{F}(\Phi, \Theta) = -\mathcal{H}[p_\Theta(\vec{z})] - \mathcal{H}[p_\Theta(\vec{x} | \vec{z})] + \frac{1}{N} \sum_{n=1}^N \mathcal{H}[q_\Phi(\vec{z}; \vec{x}^{(n)})] \quad (6)$$

$$= -\frac{D}{2} \log(2\pi e \sigma^2) + \frac{1}{2N} \sum_{n=1}^N \sum_{h=1}^H \log(\tau_h^2(\vec{x}^{(n)}; \Phi)) \quad (7)$$

where $\mathcal{H}[p(\cdot)]$ denotes the entropy of a distribution $p(\cdot)$. At convergence, the bound is according to (6) given by the entropies of prior, decoder and encoder distribution. As such, it only depends on the variance parameters of the encoder and decoder and not on any parameters of the distribution means. The second line (7) makes this dependence explicit (and note that the second term results from subtracting the prior entropy from the average entropy of the variational distributions).

Considering Eqn.7, we remark that the expression does not contain any approximations of any integrals. Using just the data points and the learned parameters, the bound can at convergence be computed exactly. We remark that the closed-form variational bound (7) does *not* replace the original bound as a learning

objective, of course (i.e., it can not be used analogously to Eqn. 4 or 5 for learning). Importantly, however, Eqn. 7 (and the generalizations we later discuss) implies that during learning the variational bound *has to* convergence to a sum of three entropies.

Related work. There is a long-standing interest in stationary points of variational lower bounds. For instance, likelihoods, lower bounds and their stationary points have been studied in detail for (restricted) Boltzmann machines (e.g. Welling and Teh, 2003), elementary generative models (e.g. Frey, 1999; Tipping and Bishop, 1999) as well as general graphical models (Freeman and Weiss, 2000; Weiss and Freeman, 2000; Yedidia et al., 2001; Opper and Saad, 2001). For deep generative networks stationary points are, consequently, likewise of high interest. For instance, Lucas et al. (Lucas et al., 2019), 2019, linked phenomena like mode collapse in VAEs to the stability of stationary points of the variational lower bound; and Dai et al. (Dai et al., 2018), 2018, analyzed a series of tractable special cases of VAEs to better understand convergence points of VAE learning. Notably both, Lucas et al. and Dai et al. emphasise the close connections of VAEs to principal component analysis (PCA). Theoretical results on different versions of PCA (e.g. Tipping and Bishop, 1999; Xu et al., 2010; Holtzman et al., 2020, for probabilistic, sparse and robust PCA) can consequently be of direct relevance for VAE research and visa versa.

Our derivations for VAEs will show that variational bounds are at convergence directly related to the entropies of those distributions that define VAEs. The relation between the integrals of the variational lower bound and entropies has been of interest previously (Lücke and Henniges, 2012). However, the main results of the previous work have used (A) the limit case of infinitely many data points, (B) assumed a perfect match of variational and full posterior distributions, and (C) required convergence to global optima. The work also discussed relaxations of these rather rigid assumptions (Lücke and Henniges, 2012, Sec. 6). But those relaxations made use of properties of sparse coding like models trained using expectation maximization. While being related, the previous results are, therefore, not applicable to the training of VAEs.

Finally, a related but different line of research discusses how *other* learning objectives for deep models can be defined that are closed-form by definition. Examples are work by Kingma and Dhariwal (Kingma and Dhariwal, 2018), 2018, or Oord et al. (Oord et al., 2016), 2016. In contrast, we here investigate the standard (in general intractable) learning objective of VAEs and show its analytical tractability at convergence.

2 Variational Lower Bounds at Convergence

For the derivation of the introductory VAE (VAE-1, defined by Eqn. 1) we will first need a more explicit form of the decoder DNN. We assume the DNN to be of standard form, i.e., the non-linearity $\vec{\mu}_\Theta(\vec{z})$ is a series of nested linear matrix multiplications followed by point-wise non-linearities:

$$\vec{\mu}_\Theta(\vec{z}) = W^{(L)} \mathcal{S}_{L-1}(\dots \mathcal{S}_0(W^{(0)} \vec{z} + \vec{b}_0) \dots) + \vec{b}_L, \quad (8)$$

where $W^{(l)}$ denotes the weight matrix of layer l and \vec{b}_l denotes its bias terms. The pointwise non-linearities $\mathcal{S}_l(\cdot)$ can differ from layer to layer. For the non-linearities that define the encoder (i.e., Eqn. 3), we will not require any further explicit forms.

2.1 A Reparametrized VAE

Before we derive Eqn. (6) for VAE-1, let us consider a different VAE which can be regarded as a reparametrization of VAE-1. It takes the following form:

Model VAE-2

$$p_\Theta(\vec{z}) = \mathcal{N}(\vec{z}; \vec{0}, A), \quad p_\Theta(\vec{x} | \vec{z}) = \mathcal{N}(\vec{x}; \vec{\mu}_\Theta(\vec{z}), \sigma^2 \mathbb{1}), \quad \text{with } A = \begin{pmatrix} \alpha_1^2 & & \\ & \ddots & \\ & & \alpha_H^2 \end{pmatrix}, \quad (9)$$

$$\text{and } q_\Phi^{(n)}(\vec{z}) = \mathcal{N}(\vec{z}; \vec{\nu}_\Phi(\vec{x}^{(n)}), \vec{\mathcal{T}}_\Phi(\vec{x}^{(n)})), \quad (10)$$

where the matrix $\tilde{\mathcal{T}}_{\Phi}(\vec{x}^{(n)})$ is defined as in Eqn. (2) but with $\tilde{\tau}_h^2(\vec{x}^{(n)}; \Phi)$ instead of $\tau_h^2(\vec{x}^{(n)}; \Phi)$ denoting the positive diagonal elements. We will assume the same decoder DNN for VAE-2 as for VAE-1 except of constraining the matrix of the first linear mapping, $\tilde{W}^{(0)}$, to have columns of unit length. Concretely, we use

$$\tilde{\mu}_{\Theta}(\tilde{z}) = W^{(L)} \mathcal{S}_{L-1}(\cdots \mathcal{S}_0(\tilde{W}^{(0)} \tilde{z} + \vec{b}_0) \cdots) + \vec{b}_L, \quad (11)$$

$$\text{where } \tilde{W}^{(0)} = (\tilde{W}_1^{(0)}, \dots, \tilde{W}_H^{(0)}) \text{ with } (\tilde{W}_h^{(0)})^T \tilde{W}_h^{(0)} = 1 \text{ for all } h. \quad (12)$$

We will later see that VAE-2 can parametrize the same distributions as VAE-1. The advantage of VAE-2 compared to VAE-1 is that it is of a form for which the variance parameters of the prior distribution can be learned (which will be exploited below).

The stationary points of VAE-2 are clearly defined. They are those points in parameter space for which the derivatives w.r.t. all parameters (parameters Θ and Φ) vanish. For VAE-2 this implies:

$$\frac{d}{d\sigma^2} \mathcal{F}(\Phi, \Theta) = 0 \quad \text{and} \quad \frac{d}{d\alpha_h^2} \mathcal{F}(\Phi, \Theta) = 0 \quad \forall h. \quad (13)$$

For VAE-2 the derivatives w.r.t. the DNN parameters $W^{(l)}$ and \vec{b}_l are also zero at stationary points as well as all derivatives w.r.t. the encoder parameters Φ (for the parameters $\tilde{W}^{(0)}$ a derivative with Lagrange multipliers is zero). However, we will below only use (13).

We can now proceed to proof the following proposition:

Proposition 1

Consider VAE-2 defined by Eqns. (9) to (12). Then at all stationary points of the variational lower bound of VAE-2 the following applies:

$$\begin{aligned} \mathcal{F}(\Phi, \Theta) &= -\mathcal{H}[p_{\Theta}(\tilde{z})] - \mathcal{H}[p_{\Theta}(\vec{x} | \tilde{z})] + \frac{1}{N} \sum_{n=1}^N \mathcal{H}[q_{\Phi}(\tilde{z}; \vec{x}^{(n)})] \\ &= -\frac{1}{2} \log(\det(2\pi e A)) - \frac{D}{2} \log(2\pi e \sigma^2) + \frac{1}{N} \sum_{n=1}^N \frac{1}{2} \log(\det(2\pi e \tilde{\mathcal{T}}_{\Phi}(\vec{x}^{(n)}))) \end{aligned} \quad (14)$$

Proof

We can rewrite the standard formulation of the variational lower bound (4) to consist of three terms:

$$\begin{aligned} \mathcal{F}(\Phi, \Theta) &= \mathcal{F}_1(\Phi, \Theta) + \mathcal{F}_2(\Phi, \Theta) + \mathcal{F}_3(\Phi), \text{ where} \\ \mathcal{F}_1(\Phi, \Theta) &= \frac{1}{N} \sum_n \int q_{\Phi}^{(n)}(\vec{z}) \log(p_{\Theta}(\vec{z})) d\vec{z} \\ \mathcal{F}_2(\Phi, \Theta) &= \frac{1}{N} \sum_n \int q_{\Phi}^{(n)}(\vec{z}) \log(p_{\Theta}(\vec{x}^{(n)} | \vec{z})) d\vec{z} \\ \mathcal{F}_3(\Phi) &= -\frac{1}{N} \sum_n \int q_{\Phi}^{(n)}(\vec{z}) \log(q_{\Phi}^{(n)}(\vec{z})) d\vec{z}, \end{aligned}$$

where we dropped the ‘tilde’ for \vec{z} for the proof.

First consider $\mathcal{F}_2(\Phi, \Theta)$ and observe that the logarithm of the prefactor $-\frac{D}{2} \log(2\pi\sigma^2)$ of $p_{\Theta}(\vec{x} | \vec{z})$ resembles the entropy of the Gaussian distribution (up to a constant factor). Hence, we can re-express $\mathcal{F}_2(\Phi, \Theta)$ as follows:

$$\begin{aligned} \mathcal{F}_2(\Phi, \Theta) &= \frac{1}{N} \sum_n \left(-\frac{1}{2\sigma^2} \int q_{\Phi}^{(n)}(\vec{z}) \|\vec{x}^{(n)} - \vec{\mu}_{\Theta}(\vec{z})\|^2 d\vec{z} - \frac{D}{2} \log(2\pi\sigma^2) - \frac{D}{2} + \frac{D}{2} \right) \\ &= \frac{D}{2} \left(1 - \frac{1}{ND\sigma^2} \sum_n \int q_{\Phi}^{(n)}(\vec{z}) \|\vec{x}^{(n)} - \vec{\mu}_{\Theta}(\vec{z})\|^2 d\vec{z} - \frac{D}{2} \log(2\pi e \sigma^2) \right), \end{aligned} \quad (15)$$

where the last term is now the negative entropy of a Gaussian (where ‘e’ is Euler’s number).

At stationary points it applies that $\frac{d}{d\sigma^2} \mathcal{F}(\Phi, \Theta) = 0$. Only $\mathcal{F}_2(\Phi, \Theta)$ depends on σ^2 , which implies $\frac{d}{d\sigma^2} \mathcal{F}_2(\Phi, \Theta) = 0$. In virtue of Eqn. (15), the derivative has a specific structure given by:

$$\begin{aligned} 0 &= \frac{d}{d\sigma^2} \mathcal{F}_2(\Phi, \Theta) = \frac{D}{2} \left(\frac{1}{ND\sigma^4} \sum_n \int q_{\Phi}^{(n)}(\vec{z}) \|\vec{x}^{(n)} - \vec{\mu}_{\Theta}(\vec{z})\|^2 d\vec{z} \right) - \frac{D}{2\sigma^2} \\ &= -\frac{D}{2\sigma^2} \left(1 - \frac{1}{ND\sigma^2} \sum_n \int q_{\Phi}^{(n)}(\vec{z}) \|\vec{x}^{(n)} - \vec{\mu}_{\Theta}(\vec{z})\|^2 d\vec{z} \right). \end{aligned}$$

As $\frac{D}{2\sigma^2}$ is greater zero, it follows that: $1 - \frac{1}{ND\sigma^2} \sum_n \int q_{\Phi}^{(n)}(\vec{z}) \|\vec{x}^{(n)} - \vec{\mu}_{\Theta}(\vec{z})\|^2 d\vec{z} = 0$.

We recognize the integral to be the first term of Eqn. (15), i.e., the term not depending on the Gaussian entropy. We can thus conclude that at stationary points of $\mathcal{F}(\Phi, \Theta)$ it applies that

$$\mathcal{F}_2(\Phi, \Theta) = -\frac{D}{2} \log(2\pi e\sigma^2) = -\mathcal{H}[p_{\Theta}(\vec{x} | \vec{z})]. \quad (16)$$

Next we consider the term $\mathcal{F}_1(\Phi, \Theta)$ of the variational lower bound. Analogous to $\mathcal{F}_2(\Phi, \Theta)$, we observe that the logarithm of the prefactor is similar to the entropy of a Gaussian (this time with diagonal covariance) and we rewrite:

$$\begin{aligned} \mathcal{F}_1(\Phi, \Theta) &= \frac{1}{N} \sum_n \left(-\sum_h \frac{1}{2\alpha_h^2} \int q_{\Phi}^{(n)}(\vec{z}) z_h^2 d\vec{z} - \frac{1}{2} \sum_h \log(2\pi\alpha_h^2) \right) \\ &= \frac{1}{2} \sum_h \left(1 - \frac{1}{N\alpha_h^2} \sum_n \int q_{\Phi}^{(n)}(\vec{z}) z_h^2 d\vec{z} \right) - \frac{1}{2} \sum_h \log(2\pi e\alpha_h^2), \end{aligned} \quad (17)$$

where the last term is the negative entropy of the prior. At stationary points Eqn. (13) applies and we obtain:

$$\begin{aligned} 0 &= \frac{d}{d\alpha_h^2} \mathcal{F}_1(\Phi, \Theta) = \frac{1}{2} \sum_{h'} \frac{\delta_{hh'}}{N\alpha_h^4} \sum_n \int q_{\Phi}^{(n)}(\vec{z}) z_{h'}^2 d\vec{z} - \frac{1}{2} \sum_{h'} \frac{\delta_{hh'}}{\alpha_h^2} \\ &= -\frac{1}{2\alpha_h^2} \left(1 - \frac{1}{N\alpha_h^2} \sum_n \int q_{\Phi}^{(n)}(\vec{z}) z_h^2 d\vec{z} \right). \end{aligned}$$

As $\frac{1}{2\alpha_h^2}$ is greater zero, it follows that for each h : $1 - \frac{1}{N\alpha_h^2} \sum_n \int q_{\Phi}^{(n)}(\vec{z}) z_h^2 d\vec{z} = 0$.

The first sum over h in Eqn. (17) is consequently zero, and we obtain at convergence:

$$\mathcal{F}_1(\Phi, \Theta) = -\frac{1}{2} \log(\det(2\pi eA)) = -\mathcal{H}[p_{\Theta}(\vec{z})]. \quad (18)$$

The term $\mathcal{F}_3(\Phi)$ is directly given as the average entropy of the variational distribution. Taken together, we thus obtain the claim (14). \square

2.2 Convergence to Sums of Entropies

We can now provide a result for the variational bounds of VAE-1 by translating the result of Prop. 1 back to the original parametrization.

Proposition 2

Consider VAE-1 defined by Eqns. (1) and (2). At all stationary points of the variational lower bound of VAE-1 it applies that:

$$\mathcal{F}(\Phi, \Theta) = \frac{1}{N} \sum_{n=1}^N \mathcal{H}[q_{\Phi}(\vec{z}; \vec{x}^{(n)})] - \mathcal{H}[p_{\Theta}(\vec{z})] - \mathcal{H}[p_{\Theta}(\vec{x} | \vec{z})] \quad (19)$$

$$= \frac{1}{2N} \sum_{n=1}^N \sum_{h=1}^H \log(\tau_h^2(\vec{x}^{(n)}; \Phi)) - \frac{D}{2} \log(2\pi e\sigma^2) \quad (20)$$

Proof

Given VAE-1, we replace the weights $W^{(0)}$ of the decoder DNN (8) as follows:

$$W^{(0)} = \tilde{W}^{(0)} A^{\frac{1}{2}} = (\alpha_1 \tilde{W}_1^{(0)}, \dots, \alpha_H \tilde{W}_H^{(0)}), \quad (21)$$

with $\tilde{W}^{(0)} = (\tilde{W}_1^{(0)}, \dots, \tilde{W}_H^{(0)})$ and A as in Eqn. (9). We take the column vectors of $\tilde{W}^{(0)}$ to be constrained to unit length as in Eqn. (12). A and $\tilde{W}^{(0)}$ parametrize the same space of matrices as W . The first linear operation of the DNN (8) now becomes:

$$W^{(0)} \vec{z} + \vec{b}_0 = \sum_h \tilde{W}_h^{(0)} \alpha_h z_h + \vec{b}_0. \quad (22)$$

Considering the term $\alpha_h z_h$, we can now generate $\tilde{z}_h \sim \mathcal{N}(\tilde{z}_h; 0, \alpha_h^2)$ instead of $z_h \sim \mathcal{N}(z_h; 0, 1)$. We recognize that VAE-1 in this way takes on the form of VAE-2 (9) to (12). Hence, when the parameters of VAE-1 represent a stationary point, the parameters with $W^{(0)}$ replaced by A and $\tilde{W}^{(0)}$ also represent a stationary point. Therefore, we can use Eqn. (14) of Prop. 1. The σ^2 remains unchanged and A could be obtained from

the column vectors of $W^{(0)}$. However, it is left to express $\tilde{\mathcal{T}}_{\Phi}(\vec{x})$ in terms of $\mathcal{T}_{\Phi}(\vec{x})$. Let us drop subscript and argument of $\tilde{\mathcal{T}}$ for readability. Then $\tilde{\mathcal{T}}$ is the covariance matrix of a Gaussian distribution defined in the space of \tilde{z} . The random variable \tilde{z} is because of Eqn. (22) given by $\tilde{z} = A^{-\frac{1}{2}}\vec{z}$. Consequently, if \tilde{z} is Gaussian distributed with covariance $\tilde{\mathcal{T}}$, then \vec{z} is Gaussian distributed with covariance $\mathcal{T} = A^{-\frac{1}{2}}\tilde{\mathcal{T}}(A^{-\frac{1}{2}})^{\top}$. As all matrices are diagonal, we get $\tilde{\mathcal{T}} = A\mathcal{T}$. Inserting into (14) we observe the first term to cancel with part of the last term:

$$\begin{aligned} \mathcal{F}(\Phi, \Theta) &= -\frac{1}{2} \log(\det(2\pi eA)) - \frac{D}{2} \log(2\pi e\sigma^2) + \frac{1}{N} \sum_n \frac{1}{2} \log(\det(2\pi eA\mathcal{T}_{\Phi}(\vec{x}^{(n)}))) \\ &= -\frac{H}{2} \log(2\pi e) - \frac{D}{2} \log(2\pi e\sigma^2) + \frac{1}{N} \sum_n \frac{1}{2} \log(\det(2\pi e\mathcal{T}_{\Phi}(\vec{x}^{(n)}))) \end{aligned} \quad (23)$$

$$= -\frac{D}{2} \log(2\pi e\sigma^2) + \frac{1}{2N} \sum_n \log(\det(\mathcal{T}_{\Phi}(\vec{x}^{(n)}))). \quad (24)$$

The middle equation we recognize as the sum of three entropies in Eqn. (19), which proves the claim. The last equation explicitly expresses the entropies (after a further simplification) using the variance parameters of VAE-1. For Eqn. (19) we moved the last term in Eqn. (23) to the front to match the order of terms to the order of processing in VAEs. \square

There are a number of implications and remarks if considering Prop. 2: As already pointed out in the introduction, no approximations of any integrals (nor any other approximations) are required. The computation of the bound is consequently very straight-forward and efficient in practice.¹ More importantly, however, is the observation that learning of VAEs (as given by VAE-1) necessarily converges to sums of entropies. As a consequence, the value of the bound only depends on a subset of VAE parameters at convergence: the variances of encoder and decoder (the entropies do not depend on the DNNs for Gaussian means). An interpretation of this result is that the goal of VAE training is to make the final variance of the decoder as small as possible while trying to keep the variances of the encoder as large as possible. Any other parameters of the VAE only affect the bound through these variances.

Linear VAEs. Standard VAEs as studied above exhibit complex learning behavior such that theoretical insights are notoriously difficult to obtain. To better understand salient challenges of VAE training such as mode collapse, a natural approach is to first try to gain insights using as elementary as possible models. For VAEs, the most elementary such model is presumably represented by a linear VAE (also compare Rumelhart et al., 1985; Baldi and Hornik, 1989; Dai et al., 2018; Kulin et al., 2019; Lucas et al., 2019), i.e., a VAE with decoder and encoder given, respectively, by:

$$p_{\Theta}(\vec{z}) = \mathcal{N}(\vec{z}; \vec{0}, \mathbb{1}), \quad p_{\Theta}(\vec{x} | \vec{z}) = \mathcal{N}(\vec{x}; W\vec{z} + \vec{\mu}_0, \sigma^2 \mathbb{1}), \quad (25)$$

$$\text{and } q_{\Phi}^{(n)}(\vec{z}) = \mathcal{N}(\vec{z}; V(\vec{x}^{(n)} - \vec{\mu}_0), \mathcal{T}), \quad \text{with covariance } \mathcal{T} = \begin{pmatrix} \tau_1^2 & & \\ & \ddots & \\ & & \tau_H^2 \end{pmatrix}. \quad (26)$$

The linear VAE is a special case of VAE-1, with linear DNNs instead of the usual deep non-linear versions. Therefore, we can conclude the following:

Corollary 1

Consider the linear VAE defined by Eqns. (25) to (26). Then at all stationary points of its variational lower bound (5) it applies that:

$$\mathcal{F}(\Phi, \Theta) = -\frac{D}{2} \log(2\pi e\sigma^2) + \frac{1}{2} \sum_{h=1}^H \log(\tau_h^2). \quad (27)$$

Proof

For the proof of Prop. 2 we only required the reparametrization of the first linear mapping of the decoder DNN (8). Prop. 2 thus also applies for the linear VAE as a special case of VAE-2 (we elaborate in Appendix A). Inserting the matrix \mathcal{T} of Eqn. (26) into Eqn. (20) directly results in the claim (27) as \mathcal{T} does not depend on n . \square

Eqn. (27) further highlights that the variance parameters determine the bound at convergence. As it is known that linear VAEs can recover the exact maximum likelihood (Dai et al., 2018; Lucas et al., 2019), we can even conclude that the bound (27) is tight at convergence. We use this result in Sec. 3 and elaborate in Appendix A.

¹We remark in this context that the DNN for the covariance of the variational distributions is in practice anyway often defined using the $\log(\tau_h^2(\vec{x}; \Phi))$.

2.3 General Standard VAEs

VAE-1 represents a very common form of VAEs. However, generalizations which use a DNN for decoder variances alongside a DNN for decoder means are widespread as well (Rezende et al., 2014; Dorta et al., 2018, etc). To cover all VAEs with standard Gaussian distributions, we hence have to extend our analysis. Consider therefore VAEs of the following form:

Model VAE-3

$$p_{\Theta}(\vec{z}) = \mathcal{N}(\vec{z}; \vec{0}, \mathbb{1}), \quad (28)$$

$$p_{\Theta}(\vec{x} | \vec{z}) = \mathcal{N}(\vec{x}; \vec{\mu}_{\Theta}(\vec{z}), \Sigma_{\Theta}(\vec{z})), \quad \text{where } \Sigma_{\Theta}(\vec{z}) = \begin{pmatrix} \sigma_1^2(\vec{z}; \Theta) & & \\ & \ddots & \\ & & \sigma_D^2(\vec{z}; \Theta) \end{pmatrix} \quad (29)$$

is diagonal with diagonal elements depending on \vec{z} . The vector defined by the diagonal elements of $\Sigma_{\Theta}(\vec{z})$ will be denoted by $\vec{\sigma}_{\Theta}^2(\vec{z}) = (\sigma_1^2(\vec{z}; \Theta), \dots, \sigma_D^2(\vec{z}; \Theta))^T$. This vector we will now take to be parametrized by a DNN, i.e., the decoder of VAE-3 uses two DNNs:

$$\vec{\mu}_{\Theta}(\vec{z}) = \text{DNN}_{\mu}(\vec{z}; W), \quad \vec{\sigma}_{\Theta}^2(\vec{z}) = \text{DNN}_{\sigma}(\vec{z}; M). \quad (30)$$

We take these two DNNs to be parametrized by two distinct sets of parameters, W and M , and both sets of parameters we take to contain all weights and biases of the respective DNN. We require both DNNs to have at least one hidden layer. The encoder we take to be the same as for VAE-1.

Because of the \vec{z} -dependence, it is obvious that Prop. 2 can not apply since a naive replacement of σ^2 in Eqn. (20), even assuming a scalar $\sigma^2(\vec{z})$, does not make sense. The proof of Prop. 2 explicitly used that σ^2 does not depend on \vec{z} , so no straight-forward generalization offers itself. However, at convergence it is still possible to derive expressions for the bound in terms of entropies:

Proposition 3

Consider VAE-3 defined by Eqns. (28) to (30) with encoder (2). At all stationary points of the variational lower bound of VAE-3 it holds that:

$$\begin{aligned} \mathcal{F}(\Phi, \Theta) &= \frac{1}{N} \sum_{n=1}^N \mathcal{H}[q_{\Phi}(\vec{z}; \vec{x}^{(n)})] - \mathcal{H}[p_{\Theta}(\vec{z})] - \frac{1}{N} \sum_{n=1}^N \mathbb{E}_{q_{\Phi}^{(n)}} \{ \mathcal{H}[p_{\Theta}(\vec{x} | \vec{z})] \} \\ &= \frac{1}{2N} \sum_{n=1}^N \sum_{h=1}^H \log(\tau_h^2(\vec{x}^{(n)}; \Phi)) - \frac{1}{2N} \sum_{n=1}^N \sum_{d=1}^D \mathbb{E}_{q_{\Phi}^{(n)}} \{ \log(\sigma_d^2(\vec{z}; \Theta)) \} - \frac{D}{2} \log(2\pi e). \end{aligned} \quad (31)$$

Proof Sketch

The proof of Prop. 3 is considerably more intricate than those for Props. 1 and 2. The main additional challenge is the integral over $\log(p_{\Theta}(\vec{x}^{(n)} | \vec{z}))$ (compare term $\mathcal{F}_2(\Theta, \Phi)$ in the proof of Prop. 1). A generalization is, however, possible using a reformulation of the integral in terms of the entropy of $p_{\Theta}(\vec{x}^{(n)} | \vec{z})$. Appendix C gives the full derivation. The generalization can be thought of as similar to the proof of Prop. 1, which was presented in a form that makes it similar to the general case of Prop. 3. Derivations for the other terms ($\mathcal{F}_1(\Theta, \Phi)$ and $\mathcal{F}_2(\Theta, \Phi)$) as well as the reparametrization are as for Prop. 1 and Prop. 2. \square

Considering Prop. 3, observe that the final result is concise and its application to a given VAE is straight-forward (while the proof is long and technical). Also observe that Eqn. (31) is indeed a generalization of Eqn. (20): if we replace $\sigma_d^2(\vec{z}; \Theta)$ by a scalar σ^2 , then we drop back to Eqn. (20). As was the case for Prop. 2, the result of Prop. 3 applies for commonly encountered conditions. For *idealized* conditions, convergence to sums of entropies as in Prop. 3 can be shown relatively easily (see, e.g., Lücke and Henniges, 2012). However, idealized would in this context mean that four unrealistic conditions have to be fulfilled: (1) the data have to be distributed according to the used generative model; (2) the data set has to be infinitely large; (3) the variational distributions have to be equal to the posterior; and (4) learning has to converge to a global optimum. In contrast, Prop. 3 states that convergence to sums of entropies also follows under realistic conditions for all standard VAEs: for any (reasonable) finite or infinite data sets, for any stationary point, and for any variational distributions. We remark that Eqn. (31) can (like Prop. 2) also be used to much more conveniently estimate the variational bound than the original bound (5) and we elaborate in Appendix B.

3 Numerical Verification

Let us now consider some numerical experiments. They will serve as a verification of our analytical results and will point to some potential applications.

Linear VAEs. The linear VAE given by Eqns. (25) and (26) allows for the most direct investigation of the result of Prop. 2. It has the advantage that we know the optimal solution in this case: it is given by the well-known maximum likelihood solution of p-PCA (Tipping and Bishop, 1999; Roweis, 1998). For the experiments we therefore first generate data according to the p-PCA generative model (details in Appendix D). In Fig. 1(a), top plot, we then compare the three entropies of Eqn. (27) with the standard lower bound (5), estimated by sampling, and the known exact log-likelihood solution (Appendix A, Eqn. 37) for the same set of data points. For verification purposes, we additionally show the ground-truth log-likelihood for the generative parameters, as well as the model log-likelihood on held-out data.

Following the proof of Prop. 1 and thus Prop. 2, the lower bound (5) and the three entropies (27) only have to be identical at stationary points of the variance parameters. This suggests that e.g. for fixed σ^2 we can not expect the lower bound to converge to the three entropies. This is shown by the dashed lines in Fig. 1(a), top plot, which shows two examples with σ^2 fixed to two suboptimal values.

Standard VAEs. To investigate more common use cases, we show in Fig. 1(b) experiments of a standard non-linear VAE (model VAE-1, in Eqn. 1 with encoder 2) on MNIST data LeCun et al. (1998). For verification of Prop. 3, we also show experiments with VAE-3 in Fig. 1(c), where we used the same PCA data as for the linear VAE but introduced an additional non-linear transformation on the data, projecting it onto a ring-like structure in the D -dimensional space (compare Doersch, 2016). Since no ground-truth log-likelihood is available for these models, we only show the standard lower bound (5), estimated by sampling, and compare it to the three entropies (20) and (31), respectively. More details and visualizations are provided in Appendix D.

Experimental Results. As can be observed, the sampled lower bound converges towards the sum of three entropies when the variance parameters are converging towards stationary points. In Fig. 1(a), top, we also see that both the lower bound and the three entropies converge to the log-likelihood (with the tight lower bound mostly invisible under the log-likelihood) and recover the ground-truth well. The gap between lower bound and three entropies might become small even before all parameters converged, as seen, e.g., in Fig. 1(c), since only zero-gradients of the variances are required, including, e.g., saddle points or saddle surfaces, which commonly occur in DNNs. When σ is fixed to a suboptimal value (Fig. 1(a), top), the assumption for Props. 1 to 3 is not fulfilled, leading to a finite gap between lower-bound and the three entropies result at convergence.

The bottom plots show the absolute difference between the sampled lower bound and the three entropies relative to the final sampled lower bound (in percent). Shown is the median over 10 runs for Fig. 1(a) and (b) and over 100 runs for Fig. 1(c) with the interquartile range as shaded area, i.e., 50% of the deviations fall within this area. At convergence, the difference between lower bound and three entropies consistently approaches zero. Small gaps we can account primarily to fluctuations caused by finite learning rates, batch sizes and numbers of samples. E.g., for VAE-3, $\sigma_d(\vec{z}; \Theta)$ has to be approximated via sampling and we confirmed that the small gap of $<0.5\%$ in Fig. 1(c), bottom, is in the order of magnitude of the sampling noise of $\sigma_d(\vec{z}; \Theta)$, which makes the three entropies fluctuate around the lower bound (see also Appendix D, Fig. 4).

4 Discussion

Stationary points of learning objectives are of central importance for our understanding of learning algorithms. Their properties are consequently frequently studied in the literature (e.g. Frey, 1999; Tipping and Bishop, 1999; Yedidia et al., 2001; Oppen and Saad, 2001; Choromanska et al., 2015; Dai et al., 2018; Lucas et al., 2019). Here we focused on VAEs and the stationary points of their variational lower bounds. Although VAEs can involve intricate DNNs, we here report an exact theoretical result: at all stationary points the variational lower bound is identical to a sum of three entropies. The result does notably not require any idealized and unrealistic conditions. It applies precisely also under those conditions met when standard VAEs are applied in practice: finite data sets, imperfect matches of generative models to data, and at local optima or saddle points. All derived results notably also apply for encoder distributions which imperfectly match the true posteriors. We are neither aware of any results similar to those of Props. 2 and 3 for VAEs, nor about any

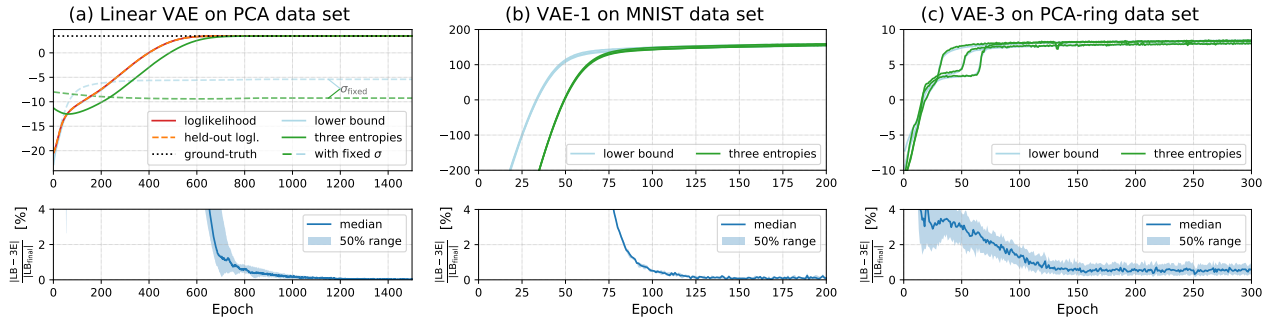


Figure 1: VAE models of increasing complexity (left to right: linear VAE, VAE-1 and VAE-3) on different data sets. **Top plots:** Absolute values of the given bounds per data point of single runs. In (a) the lower bound is barely visible as it is covered by the log-likelihood (zoom in to see). **Bottom plots:** Median and interquartile range of the relative difference between the lower bound and the three entropy formulas for the respective VAEs over multiple runs. Appendix C for more details.

discussions that VAEs may converge to sums of entropies under commonly encountered conditions. Knowing the results of Props. 2 and 3, it is conceivable that alternative and potentially less technical proofs can be found, we believe. And such proofs may add further theoretical insights. Future work may also focus on generalizing Prop. 3 still further. VAEs defined by Gaussian distributions are by far the most wide-spread, which makes the here derived results cover very large parts of VAE research. Other, non-Gaussian VAEs have also been of interest, however. For some VAEs (e.g., with discrete latents Rolfe, 2016; Van Den Oord et al., 2017; Khoshaman et al., 2018; Sadeghi et al., 2019; Vahdat et al., 2018; Lorberbom et al., 2019) our proofs suggest that relatively straight-forward generalizations are possible. For others (e.g. VAEs with non-Gaussian observables) derivations will presumably require significant future efforts.

Our main contributions are Propositions 1 to 3, their proofs, and consequently the observation that variational bounds of VAEs converge to sums of entropies. Different use cases (both theoretical and practical) are conceivable based on the main results. We will discuss some examples below but such examples should not distract from the contents of the propositions themselves. The theoretical content is what we here report as main result in its own right. The following list of example use cases should also not be regarded as exhaustive:

Variance parameters. One direct observation that can be derived from Props. 2, 3 and Corollary 1 is the crucial role played by the variance parameters. For VAE-1, for instance, knowing the variance parameters at convergence means knowing the value of the bound (computable in closed-form); for linear VAEs not even the data is required to estimate the bound’s value if the variance parameters are known (Eqn. 27). An example of a further theoretical analysis is discussed in Appendix B, where we show that the average posterior emerges as the natural counterpart of the data distribution in a symmetric expression of the bound. An example of practical relevance is the application of Props. 2, 3 and Corollary 1 for streaming applications and model selection where the exceedingly easy to compute expressions of the bound can be exploited – we briefly discuss in Appendix A. Also see our empirical analysis of the bounds in the vicinity of stationary points in Appendix D in this respect.

Optimization landscape. While Props. 2, 3 do allow for comparisons of the value of the bound at all stationary points, they by themselves do not define the optimization landscape (as stressed in the introduction). Consequently, the here derived bounds can not directly be used for stability analyses (which has been the focus for other contributions (Weiss and Freeman, 2000; Yedidia et al., 2001; Oppen and Saad, 2001; Welling and Teh, 2003; Dai et al., 2018; Lucas et al., 2019)). However, note that at closer inspection, the expressions derived for Props. 2 and 3 only require convergence from a subset of parameters (compare Eqn. 13 for VAE-1). The here derived expressions are consequently valid also in submanifolds of the parameter space. Future work could exploit the observation and analyze the optimization landscape within such submanifold, e.g., using solutions for those parameters for which convergence is required (and note that for VAE-1 solutions for α_h and σ^2 can be derived).

Posterior collapse. Posterior collapse is an empirically observed phenomenon: a subset of VAE latents ceases to participate in encoding and decoding; instead they assume a high variance. The mathematical mechanism of this phenomenon is ‘not well understood’ (see (Lucas et al., 2019) who also point to related empirical studies). Props. 2 and 3 can directly contribute to answering the question *why* posterior collapse happens: if a given latent can not significantly improve the decoding quality, the decoding entropy does significantly decrease with

the latent value; considering the propositions, it is then preferable for the latent to assume a high posterior variance in order to realize a high value of the bound. In other words, Props. 2 and 3 show that high entropies of encoders are advantageous as long as they outweigh increases of decoder entropies. On a more technical side, Props. 2 and 3 also suggest a measure for the degree of posterior collapse in the form of prior entropy minus average encoder entropy (the measure can be interpreted as distance to posterior collapse). Such a definition could replace, e.g., the previous ad-hoc measure based on thresholding the KL-divergence ((Lucas et al., 2019), p. 7), and would be more general.

References

- Z. Allen-Zhu and Y. Li. First efficient convergence for streaming k-PCA: a global, gap-free, and near-optimal rate. In *58th Annual Symposium on Foundations of Computer Science (FOCS)*, pages 487–492, 2017.
- P. Baldi and K. Hornik. Neural networks and principal component analysis: Learning from examples without local minima. *Neural Networks*, 2(1):53–58, 1989.
- D. M. Blei, A. Kucukelbir, and J. D. McAuliffe. Variational inference: A review for statisticians. *Journal of the American Statistical Association*, 112(518):859–877, 2017.
- A. Choromanska, Y. LeCun, and G. B. Arous. Open problem: The landscape of the loss surfaces of multilayer networks. In *Conference on Learning Theory*, pages 1756–1760. PMLR, 2015.
- C.-N. Chou and M. B. Wang. ODE-inspired analysis for the biological version of Oja’s rule in solving streaming PCA. In *Conference on Learning Theory*, pages 1339–1343. PMLR, 2020.
- B. Dai, Y. Wang, J. Aston, G. Hua, and D. Wipf. Connections with robust PCA and the role of emergent sparsity in variational autoencoder models. *The Journal of Machine Learning Research*, 19(1):1573–1614, 2018.
- C. Doersch. Tutorial on variational autoencoders. *arXiv preprint arXiv:1606.05908*, 2016.
- G. Dorta, S. Vicente, L. Agapito, N. D. Campbell, and I. Simpson. Training VAEs under structured residuals. *arXiv preprint arXiv:1804.01050*, 2018.
- W. Freeman and Y. Weiss. On the fixed points of the max-product algorithm. *IEEE Trans. on Info. Theory*, 2000.
- B. Frey. Turbo factor analysis. *Adv. Neural Information Processing*, 1999.
- G. Holtzman, A. Soffer, and D. Vilenchik. A greedy anytime algorithm for sparse pca. In *Conference on Learning Theory*, pages 1939–1956. PMLR, 2020.
- A. Khoshaman, W. Vinci, B. Denis, E. Andriyash, H. Sadeghi, and M. H. Amin. Quantum variational autoencoder. *Quantum Science and Technology*, 4(1):014001, 2018.
- D. P. Kingma and P. Dhariwal. Glow: Generative flow with invertible 1x1 convolutions. In *Advances in Neural Information Processing Systems*, pages 10215–10224, 2018.
- D. P. Kingma and M. Welling. Auto-encoding variational bayes. In *ICLR*, 2014.
- D. Kunin, J. M. Bloom, A. Goeva, and C. Seed. Loss landscapes of regularized linear autoencoders. *arXiv preprint arXiv:1901.08168*, 2019.
- Y. LeCun, L. Bottou, Y. Bengio, and P. Haffner. Gradient-based learning applied to document recognition. *Proceedings of the IEEE*, 86(11):2278–2324, 1998.
- G. Lorberbom, A. Gane, T. Jaakkola, and T. Hazan. Direct optimization through arg max for discrete variational auto-encoder. In *Advances in Neural Information Processing Systems*, pages 6203–6214, 2019.
- J. Lucas, G. Tucker, R. B. Grosse, and M. Norouzi. Don’t blame the ELBO! A linear VAE perspective on posterior collapse. In *Advances in Neural Information Processing Systems*, pages 9408–9418, 2019.

- J. Lücke and M. Henniges. Closed-form entropy limits - A tool to monitor likelihood optimization of probabilistic generative models. In *Proc. AISTATS*, pages 731–740. PMLR, 2012.
- R. Neal and G. Hinton. A view of the EM algorithm that justifies incremental, sparse, and other variants. In *Learning in Graphical Models*. Kluwer, 1998.
- A. V. Oord, N. Kalchbrenner, and K. Kavukcuoglu. Pixel recurrent neural networks. In *Proceedings of the International Conference on Machine Learning*, pages 1747–1756, 2016.
- M. Opper and D. Saad. *Advanced mean field methods: Theory and practice*. MIT press, 2001.
- D. J. Rezende, S. Mohamed, and D. Wierstra. Stochastic backpropagation and approximate inference in deep generative models. In *ICML*, 2014.
- J. T. Rolfe. Discrete variational autoencoders. *arXiv preprint arXiv:1609.02200*, 2016.
- S. T. Roweis. EM algorithms for PCA and SPCA. In *Advances in Neural Information Processing Systems*, pages 626–632, 1998.
- D. E. Rumelhart, G. E. Hinton, and R. J. Williams. Learning internal representations by error propagation. Technical report, California Univ San Diego La Jolla Inst for Cognitive Science, 1985.
- H. Sadeghi, E. Andriyash, W. Vinci, L. Buffoni, and M. H. Amin. PixelVAE++: Improved PixelVAE with discrete prior. *arXiv preprint arXiv:1908.09948*, 2019.
- M. Tipping and C. Bishop. Probabilistic principal component analysis. *Journal of the Royal Statistical Society. Series B*, 61, 1999.
- A. Vahdat, W. G. Macreedy, Z. Bian, A. Khoshaman, and E. Andriyash. DVAE++: Discrete variational autoencoders with overlapping transformations. *arXiv:1802.04920*, 2018.
- A. Van Den Oord, O. Vinyals, et al. Neural discrete representation learning. In *Advances in Neural Information Processing Systems*, pages 6306–6315, 2017.
- Y. Weiss and W. T. Freeman. Correctness of belief propagation in Gaussian graphical models of arbitrary topology. In *Advances in Neural Information Processing Systems*, pages 673–679, 2000.
- M. Welling and Y. W. Teh. Approximate inference in Boltzmann machines. *Artificial Intelligence*, 143(1): 19–50, 2003.
- H. Xu, C. Caramanis, and S. Mannor. Principal component analysis with contaminated data: The high dimensional case. In *Conference on Learning Theory*, 2010.
- J. S. Yedidia, W. T. Freeman, and Y. Weiss. Generalized belief propagation. In *Advances in Neural Information Processing Systems*, pages 689–695, 2001.

Appendix

While Props. 2 and 3 represent by themselves theoretical results, it may be of interest to discuss different potential use cases. Here we, therefore, elaborate on those cases mentioned in the discussion.

The special role of *variance parameters* to determine the bound is relevant both for practical as well as for theoretical considerations. An example for potential practical relevance is discussed in Appendix A below, which is itself referring to Appendix D for further numerical verifications. An example in which the role of variance parameters is further investigated theoretically is discussed in Appendix B. As variance parameters define the here discussed entropies, they will be of central relevance throughout the discussed use cases.

Optimization landscape. To elaborate on the application of the results for the analysis of VAE optimization landscapes, consider first VAEs of type VAE-1 (Eqns. 1 to 3). For such VAEs the closed-form bound of Prop. 2 applies at all stationary points. The result was notably derived using properties of two types of variance parameters: decoder variance and prior variance. Importantly, the prior variance is in the usual parametrization of VAEs not part of the prior but part of the decoder DNN, i.e., the α_h are part of the first DNN layer (see VAE-2 for an explicit encoding with prior variance). While Eqn. (20) of Prop. 2 does by itself not describe an optimization landscape, we can recover a description of an optimization landscape if we insert solutions for α_h^2 for σ^2 into Eqn. (20). Solutions for α_h and σ^2 are given by the following explicit functions:

$$\alpha_h^2 = \frac{1}{N} \sum_{n=1}^N \int q_{\Phi}(\vec{z}; \vec{x}^{(n)}) z_h^2 d\vec{z}, \quad \sigma^2 = \frac{1}{DN} \sum_{n=1}^N \int q_{\Phi}(\vec{z}; \vec{x}^{(n)}) \|\vec{x}^{(n)} - \vec{\mu}_{\Theta}(\vec{z})\|^2 d\vec{z}, \quad (32)$$

and the α_h^2 expression further simplifies for diagonal covariances. After the solutions for α_h and σ^2 are inserted into Eqn. (20), the resulting expression describes the optimization landscape within submanifolds of the parameter space (Fig. 2 shows an illustration). The description of the optimization landscape within submanifolds can be used to study the optimization landscape of the whole parameter space. We relate to posterior collapse as an example below.

Similar approaches can be used for more general VAEs but an analysis necessarily becomes more intricate, e.g., because of the dependence of decoder variances on the latents for VAEs of type VAE-3 (but note similar properties for α_h).

Posterior Collapse. Props. 2 and 3 can contribute to better understand posterior collapse, i.e., the propositions allow a contribution to the question *why* some latent variables sometimes cease to participate in encoding/decoding and instead assume a high variance. Considering Prop. 2, for instance, we can use expression $\tilde{\mathcal{F}}(\Phi, \Theta)$, which is equal to Eqn. (19) of Prop. 2 without the prior entropy (as the prior entropy is a constant):

$$\tilde{\mathcal{F}}(\Phi, \Theta) = \frac{1}{N} \sum_{n=1}^N \mathcal{H}[q_{\Phi}(\vec{z}; \vec{x}^{(n)})] - \mathcal{H}[p_{\Theta}(\vec{x} | \vec{z})] = \bar{\mathcal{H}}[q_{\Phi}^{\text{enc}}] - \mathcal{H}[p_{\Theta}^{\text{dec}}], \quad (33)$$

where $\bar{\mathcal{H}}[q_{\Phi}^{\text{enc}}]$ and $\mathcal{H}[p_{\Theta}^{\text{dec}}]$ are abbreviations for encoder entropy $\mathcal{H}[q_{\Phi}(\vec{z}; \vec{x}^{(n)})]$ and decoder entropy $\mathcal{H}[p_{\Theta}(\vec{x} | \vec{z})]$, respectively. The expression $\tilde{\mathcal{F}} = \bar{\mathcal{H}}[q_{\Phi}^{\text{enc}}] - \mathcal{H}[p_{\Theta}^{\text{dec}}]$ contains the entropies as two competing terms. The bound gets larger if we *decrease* the decoder entropy (which essentially measures a reconstruction error). But the bound also gets larger if we *increase* the encoder entropy. For the standard choice of a Gaussian encoder distribution with diagonal covariance, the encoder entropy decomposes into a sum:

$$\bar{\mathcal{H}}[q_{\Phi}^{\text{enc}}] = \mathcal{H}[q_{\Phi}(\vec{z}; \vec{x}^{(n)})] = \sum_{h=1}^H \mathcal{H}[q_{\Phi}(z_h; \vec{x}^{(n)})]. \quad (34)$$

Now suppose that values of a latent variable z_{h_o} are not (or little) contributing to decrease the decoder entropy, i.e., the latent values do not help very much in reconstructing data points. Then increasing the encoder entropy $\mathcal{H}[q_{\Phi}(z_{h_o}; \vec{x}^{(n)})]$ becomes the best strategy to obtain high values of the bound.

The expression (33) or the full three entropy expression (19) are by themselves only instructive about the relative heights of the local optima of the variational bound. However, if combined with above considerations on optimization landscapes, we can go one step further. By inserting² the expressions (32) into (33), we

²A VAE-1 can be regarded as being reparametrized as VAE-2 first. In the conventional VAE-1 form, the converged α_h can be taken as implicit in the decoder weights.

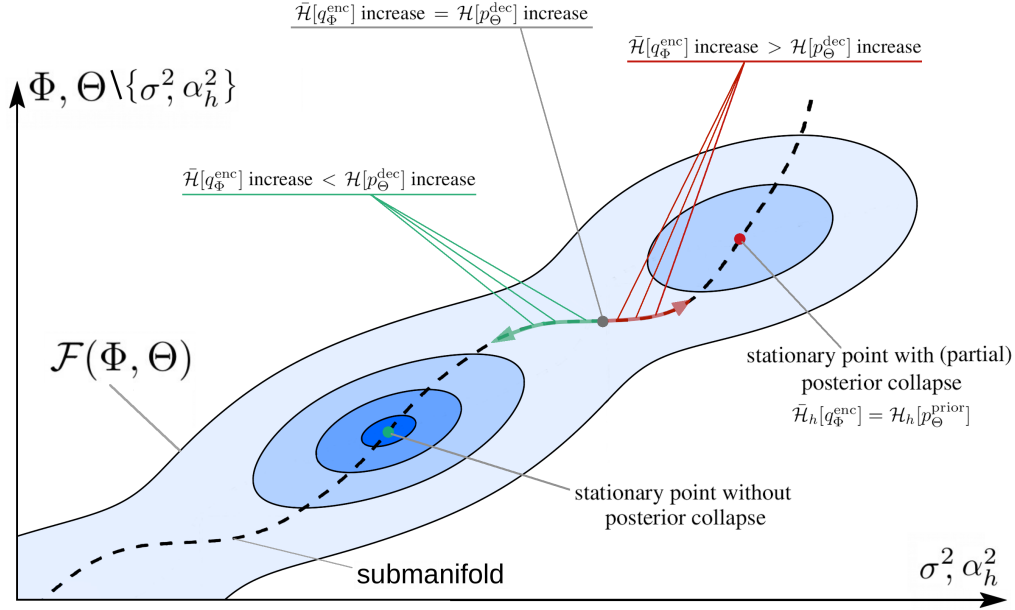


Figure 2: Visualization of the variational lower bound and its relation to the three entropies expression. The figure shows a two dimensional visualization with the following axes: the x-axis represents the hyperplane of variance parameters α_1^2 to α_H^2 together with decoder variance σ^2 . We assume a VAE of type VAE-1 for the figure. The α_1^2 to α_H^2 we take to be implicitly defined by the decoder weights (compare VAE-2). The dotted black line represents a submanifold in which the parameters of the x-axis have converged. Within the submanifold, the variational lower bound is equal to a sum of three entropies (Prop. 2). In the illustrated example, the submanifold connects a stationary point without posterior collapse to a stationary point with (partial) posterior collapse. If we start at the high local optimum and traverse the submanifold from left to right then both entropies will (tend to) increase. In the beginning, close to the high local optimum, the increase of the encoder entropy will be smaller than the increase of the decoder entropy (i.e., the derivative of $\tilde{\mathcal{F}}(\Phi, \Theta)$ is negative). Gradient ascent would consequently converge back to the high optimum (thereby decreasing $\mathcal{H}[p_\Theta^{\text{dec}}]$ as desired; green arrow). If we go further downhill, however, a turning point is reached when the encoder’s entropy increase becomes equal to the decoder’s entropy increase. To the right of the turning point, the increase of the encoder entropy outweighs the increase of the decoder entropy. As the derivative of $\tilde{\mathcal{F}}(\Phi, \Theta)$ is now positive, gradient ascent results in large increases of encoder entropy $\tilde{\mathcal{H}}[q_\Phi^{\text{enc}}]$ (1st term of $\tilde{\mathcal{F}}(\Phi, \Theta)$): the posterior collapses to high variance (red arrow). The collapsed latents will have their influence on the decoding suppressed as this avoids high decoder entropies (2nd term of $\tilde{\mathcal{F}}(\Phi, \Theta)$). At the local optimum with (partly) collapsed posterior, the encoder entropy, $\tilde{\mathcal{H}}_h[q_\Phi^{\text{enc}}]$, of a collapsed latent h will be equal to the prior entropy, $\mathcal{H}_h[p_\Theta^{\text{prior}}] := \mathcal{H}[p_\Theta(z_h)]$. Thanks to Sebastian Salwig for help with the figure.

obtain a description of the optimization landscape within a submanifold in parameter space (see dotted line of Fig. 2). The submanifold in the figure connects an optimum without posterior collapsed latents to an optimum with (partial) posterior collapse. When traversing from one optimum to the other along the submanifold, a saddle point will be reached. On the one side of the saddle point, gradient learning does decrease decoder entropy (as desired for representation learning; green arrow in Fig. 2); on the other side of the saddle point, encoder entropy of a given latent will increase (the posterior of the latent starts to collapse; red arrow in Fig. 2). Because of the latent’s increase to high entropy, removing its influence on decoding is then a plausible consequence. Otherwise, the increasingly high entropy would increase the decoder entropy and, therefore, would decrease the bound. In other words: Learning changes encoder entropy and decoder entropy. If changes of encoder entropy start to dominate changes in decoder entropy, the posterior collapses (see Fig. 2). Eqn. 33 (or Prop. 2) shows that entropies naturally emerge in contexts such as posterior collapse.

The treatment of VAEs of type VAE-3 would be similar but, for instance, $\mathcal{H}[p_\Theta^{\text{dec}}]$ would have to be replaced by $\frac{1}{N} \sum_{n=1}^N \mathbb{E}_{q_\Phi^{(n)}} \{ \mathcal{H}[p_\Theta(\vec{x} | \vec{z})] \}$ (the last term of Prop. 3).

On a more practical side, Props. 2 and 3 can also be used to directly quantify the degree of posterior collapse. Using the above insights we could define:

$$\Delta^{\text{post. collapse}} = \mathcal{H}[p_\Theta(\vec{z})] - \frac{1}{N} \sum_{n=1}^N \mathcal{H}[q_\Phi(\vec{z}; \vec{x}^{(n)})] \quad (35)$$

as a measure (note that $\mathcal{H}[p_\Theta(\vec{z})]$ is now the constant prior entropy). If all latent variables approach a variance equal to the prior variance then $\Delta^{\text{post. collapse}}$ approaches zero. If latent variables have a lower variance (i.e., lower encoder entropy) then $\Delta^{\text{post. collapse}}$ is positive.

Quantifying posterior collapse has been of interest previously. E.g., see (Lucas et al., 2019) for references to empirical studies on posterior collapse. The paper (Lucas et al., 2019) itself introduces a measure for posterior collapse based on the KL-divergence ((Lucas et al., 2019), p.7), which is then thresholded to determine if a latent has collapsed. Compared to (35) the previous measure is more ad-hoc and requires hand-set parameters for the threshold. The measure (35) may consequently be perceived as more natural, and it is more general as well: VAE encoders with non-diagonal covariance matrices can directly be treated, for instance. In case we maintain diagonal covariances, the entropies in (35) further decompose into sums, such that measures for the individual posterior collapse per latent are directly obtained in the following form:

$$\Delta_h^{\text{post. collapse}} = \mathcal{H}[p_{\Theta}(z_h)] - \frac{1}{N} \sum_{n=1}^N \mathcal{H}[q_{\Phi}(z_h; \vec{x}^{(n)})] \quad (36)$$

All above considerations can be generalized to more intricate VAEs of type VAE-3 more or less directly but individual aspects will be partly more intricate.

Appendix A: Linear VAEs and Streaming Applications

For the proof of Corollary 1 note that for the linear DNN of the decoder (i.e. for the matrix multiplication) of Eqn. 25 the same reparametrization is possible as was used for VAE-1 (i.e., using \tilde{W} with constraint columns instead of W in Eqn. 25). Furthermore, no conditions were imposed on the encoder DNN for Prop. 2, and the used properties of the stationary points (13) are the same for the linear VAE as for the VAEs above. Prop. 2 consequently applies for the linear VAE as a special case of VAE-1.

The result of Corollary 1 then highlights some properties of the variational bound at convergence. First, note that the variational bound at the stationary points can be computed efficiently and solely based on the variance parameters σ^2 and τ_h^2 . For linear VAEs, the bound is even independent of the data points, i.e., just the $H + 1$ variance parameters determine its value. In addition to this simplification, the linear VAE has a further property that makes it interesting from a theoretical perspective. Linear VAEs can be used to recover the maximum likelihood solution (compare Dai et al., 2018; Lucas et al., 2019) of probabilistic PCA (p-PCA). Lucas et al. (Lucas et al., 2019), for instance, showed that no stable stationary points of the variational lower bound exist other than the global maximum. Training of the linear VAE will thus always converge to the global maximum of the lower bound. Second, they showed that the linear encoder is flexible enough to finally recover full posteriors exactly, which makes the variational lower bound tight at convergence. As the decoder is identical to the generative model of p-PCA (Tipping and Bishop, 1999), the linear VAE thus converges to recover the optimal p-PCA likelihood. According to Corollary 1 it thus applies that after convergence of the linear VAE, Eqn. (27) is equal to the p-PCA log-likelihood.

We can combine the earlier results (e.g. Tipping and Bishop, 1999; Lucas et al., 2019) with Corollary 1 and obtain the following.

Corollary 2

Consider the linear VAE defined by Eqns. (25) and (26) with decoder parameters $\Theta = (\sigma^2, W, \vec{\mu}_0)$. Then after convergence, the parameters $(\sigma^2, W, \vec{\mu}_0)$ represent the maximum likelihood solution for p-PCA, and the value of the log-likelihood $\mathcal{L}(\Theta)$ is given by:

$$\mathcal{L}(\Theta) = -\frac{D}{2} \log(2\pi e\sigma^2) + \frac{1}{2} \sum_h \log(\tau_h^2), \quad (37)$$

where τ_h^2 are the learned variances of the VAE encoder.

Proof

As Eqn. (27) applies for all stationary points, it also applies for the global maximum of the variational lower bound. At the global maximum, the variational bound is equal to the p-PCA log-likelihood (result by Lucas et al., 2019), which proves the claim. \square

Other than for standard non-linear VAEs, the existence of a closed-form result is itself not surprising for the linear VAE. The linearities make analytic solutions of the integrals of the variational bound possible. Indeed,

we can instead of Eqn. (37) simply use the well-known closed-form solution of the p-PCA likelihood (Tipping and Bishop, 1999):

$$\mathcal{L}(\Theta) = -\frac{D}{2} \log(2\pi) - \frac{1}{2} \log(\det(C)) - \frac{1}{2} \text{Tr}(C^{-1}S), \quad (38)$$

$$\text{where } C = WW^T + \sigma^2 \mathbb{1} \quad \text{and where } S = \frac{1}{N} \sum_n (\vec{x}^{(n)} - \vec{\mu})(\vec{x}^{(n)} - \vec{\mu})^T$$

is the data covariance matrix. At convergence, we thus have two alternatives to compute the log-likelihood: Eqn. (38) and Eqn. (37). The two expressions differ, however. While both are closed-form, the well-known p-PCA likelihood (38) requires the data in the form of the data covariance matrix S . And even neglecting the computational effort to compute S , the computation of (38) is much more expensive than computing (37): For $\mathcal{L}(\Theta)$ the inverse and the determinant of the $D \times D$ matrix C have to be computed. In contrast, for the computation of $\mathcal{F}(\Phi, \Theta)$ in (37) no such computations nor data is required (although we require a linear VAE that has sufficiently converged). The derived result of Eqn. (37) can therefore be of theoretical and practical relevance especially considering the exceptionally widespread use of PCA in Machine Learning, Statistics and beyond.

Streaming Applications. One concrete practical example is PCA applied to streaming data, which is an increasingly common setting especially in recent years. In such a setting the application of a linear VAE is straight-forward, and it can be operated as alternative or in parallel to other PCA algorithms. As such a linear VAE is related to streaming PCA approaches, e.g., Allen-Zhu and Li (Allen-Zhu and Li, 2017) for an overview and Chou and Wang (Chou and Wang, 2020) for a recent example. For streaming data (as for other data) the value of the likelihood itself can be of high interest, e.g., to monitor the fit to the data or for the selection of PCA dimensions. In this context, Eqn. (37) provides an exceedingly easy way to compute the log-likelihood value. Also if the streamed data changes, the parameters of the linear VAE will change and Eqn. (37) can be used to track the changes of the likelihood without any effort. No data has to be kept in memory and no costly computations are required.

For the purposes of this paper, our first numerical experiments will use the linear VAE (Appendix D). The result can then directly be compared to the well known closed-form log-likelihood (38) as well as to sampling based approximations of the variational lower bound. Appendix D will also show empirically that the derived three entropy expressions match the lower bound with high accuracy also in vicinities of stationary points that are reached in practice.

Of course, also non-linear VAEs can and are frequently applied in streaming settings. For the non-linear case, Prop. 2 provides, for instance, an estimate of the log-likelihood in terms of a variational bound. The estimate can then be used to monitor changes in the data stream or for model selection in place of the log-likelihoods for linear VAEs. Considering (20) of Prop. 2, we now do need to take the data points into account to compute the value of the variational bound. As for the case when using the original variational bound (5), the computation of running averages across data points can be used in streaming settings. In contrast to the original expression (5), however, Prop. 2 allows for the computation of the bound in closed-form which is computationally much less demanding. Also, just one of the three DNNs which define a VAE of type VAE-1 is required (the DNN for the encoder variances). Appendix D shows that also the three entropies expression for non-linear VAEs does well approximates the original expression (5) in practically reached vicinities of stationary points.

Appendix B: Prop. 3 and dependence on variance parameters

The expression (31) is in general not closed-form. However, the intractable integral only involves the DNN for the decoder variances. The dependence on entropies at stationary points as stated in Prop. 3 does again point to the key role played by the variance parameters: the entropies themselves do not depend on the DNNs for encoder or decoder means. However, the result of Prop. 3 differs from Prop. 2. Because of the expectation value w.r.t. the encoder $q_{\Phi}^{(n)}$ the bound at convergence does (in contrast to Prop. 2) also depend on the encoder DNN for the mean. We can shed more light on this dependence by observing that the average expectation w.r.t. $q_{\Phi}^{(n)}$ is actually an expectation w.r.t. one average distribution, i.e., the middle term of Eqn. (31) is equal to:

$$-\frac{1}{2} \sum_{d=1}^D \mathbb{E}_{\bar{q}_{\Phi}} \{ \log(\sigma_d^2(\vec{z}; \Theta)) \}, \quad \text{with } \bar{q}_{\Phi} = \frac{1}{N} \sum_n q_{\Phi}^{(n)}. \quad (39)$$

If $q_{\Phi}^{(n)}$ models the true posteriors of the model well, the average posterior converges (for many data points) to the prior $p_{\Theta}(\vec{z})$. Consequently, the dependence on the DNN for the encoder *mean* disappears asymptotically for optimal $q_{\Phi}^{(n)}$ (and many data points). In that case, we recover (as for Prop. 2) that the value of the variational bound at convergence only depends on parameters for encoder and decoder variances.

Finally, note that Prop. 3 reflects the encoder and decoder parts of the lower bound more symmetrically than was apparent from Prop. 2 (only the expectation value of the middle term seems to break the symmetry). We may therefore be motivated to derive still more symmetric expressions. To do so, let us interpret the arguments of the logarithms of (31) as volumes covered by encoder and decoder distributions:

$$z\text{-Vol}(\vec{x}; \Phi) = \prod_{h=1}^H (2\tau_h(\vec{x}; \Phi)), \quad x\text{-Vol}(\vec{z}; \Theta) = \prod_{d=1}^D (2\sigma_d(\vec{z}; \Theta)). \quad (40)$$

$z\text{-Vol}(\vec{x}; \Phi)$ is a measure of the volume covered by the encoder Gaussian $q_{\Phi}^{(n)}(\vec{z})$ in latent space (\vec{z} -space). Here we used a hyper-rectangle with two standard deviations edge length to define the volume. Analogously $x\text{-Vol}(\vec{z}; \Theta)$ is the volume covered by the decoder distribution. If we now consider the limit of many data points, we arrive at a very symmetrical expression:

Corollary 3

Consider VAE-3 and let us denote by $p(\vec{x})$ the true data distribution. Then in the limit of many data points $N \rightarrow \infty$, it applies at convergence that

$$\mathcal{F}(\Phi, \Theta) = \mathbb{E}_{p(\vec{x})} \{ \log(z\text{-Vol}(\vec{x}; \Phi)) \} - \mathbb{E}_{\bar{q}_{\Phi}(\vec{z})} \{ \log(x\text{-Vol}(\vec{z}; \Theta)) \} + \text{const.} \quad (41)$$

Proof

We use $\frac{1}{N} \sum_n f(\vec{x}^{(n)}) \rightarrow \int p(\vec{x})f(\vec{x})d\vec{x}$ in the limit. Then elementary rearrangements of terms. The constant in (41) for the volume definitions (40) is given by $\text{const.} = (D - H) \log(2) - (D/2) \log(2\pi e)$. \square

The definition of volumes covered by encoder and decoder distributions may seem a bit arbitrary. Instead of Eqn. (40) one could, e.g., have defined the volumes as those rectangles containing say 50% or 90% of a distribution’s mass. Eqn. (41) does not change when changing the volume definitions, though. It is only important that $z\text{-Vol}(\vec{x}; \Phi)$ and $x\text{-Vol}(\vec{z}; \Theta)$ are measures of the covered volume. Any proportionality factors are simply changing the constant in Eqn. (41).

Considering Corollary 2, a VAE can thus be regarded as trying to balance two terms to achieve a high lower bound: it tries to make the log-volumes covered by its encoder distribution as large as possible while trying to make the log-volumes covered by its decoder distributions as small as possible. Corollary 2 may be used to analyze properties of optimal VAE solution, e.g., in terms of curvatures of data manifolds.

Appendix C: Proof of Proposition 3

We have deliberately stated the proof of Props. 1 and 2 in a form that, we hope, makes the relatively intricate and long proof of Prop. 3 easier to follow. As a prelude, observe that in the proof of Prop. 1 the reformulation of $\mathcal{F}_2(\Phi, \Theta)$ in Eqn. (15) is a key step: we formulate $\mathcal{F}_2(\Phi, \Theta)$ in terms of an entropy plus an additional term which converges to zero at stationary points. Derivatives w.r.t. σ^2 of entropy and the other term of Eqn. (15) resulted in a factorization of $\mathcal{F}_2(\Phi, \Theta)$, which allowed for deriving convergence to an entropy. For scalar σ^2 alternative proofs for the convergence to entropies may be conceivable. For the generalization of the proof for more general VAEs, we will best make use of a generalization of the expression Eqn. (15) used for the proof of Prop. 1. As for the proof of Prop. 1, we consider separately the three terms of the variational bound $\mathcal{F}(\Phi, \Theta)$:

$$\mathcal{F}(\Phi, \Theta) = \mathcal{F}_1(\Phi, \Theta) + \mathcal{F}_2(\Phi, \Theta) + \mathcal{F}_3(\Phi). \quad (42)$$

For \vec{z} -dependent decoder variances, the main difference to Prop. 1 lies in the term $\mathcal{F}_2(\Phi, \Theta)$, which is given for VAE-3 by:

$$\mathcal{F}_2(\Phi, \Theta) = \frac{1}{N} \sum_{n=1}^N \sum_{d=1}^D \int q_{\Phi}^{(n)}(\vec{z}) \log(\mathcal{N}(x_d^{(n)}; \mu_d(\vec{z}; \Theta), \sigma_d^2(\vec{z}; \Theta))) d\vec{z}$$

We now use the parametrization of the Gaussian in terms of its natural parameters $\vec{\eta}$ (of the exponential family), which will turn out to be convenient:

$$\mathcal{F}_2(\Phi, \Theta) = \frac{1}{N} \sum_{n=1}^N \sum_{d=1}^D \int q_{\Phi}^{(n)}(\vec{z}) \left(\vec{\eta}_d^{\top}(\vec{z}; \Theta) \vec{T}(x_d^{(n)}) - A(\vec{\eta}_d(\vec{z}; \Theta)) - \frac{1}{2} \log(2\pi) \right) d\vec{z} \quad (43)$$

where

$$\vec{\eta}_d(\vec{z}; \Theta) = \begin{pmatrix} \frac{\mu_d(\vec{z}; \Theta)}{\sigma_d^2(\vec{z}; \Theta)} \\ -\frac{1}{2\sigma_d^2(\vec{z}; \Theta)} \end{pmatrix}, \quad \vec{T}(x_d^{(n)}) = \begin{pmatrix} x_d^{(n)} \\ (x_d^{(n)})^2 \end{pmatrix}, \quad (44)$$

$$A(\vec{\eta}_d(\vec{z}; \Theta)) = -\frac{(\eta_d^{(1)}(\vec{z}; \Theta))^2}{4\eta_d^{(2)}(\vec{z}; \Theta)} - \frac{1}{2} \log(-2\eta_d^{(2)}(\vec{z}; \Theta)), \quad (45)$$

and where $-\frac{1}{2} \log(2\pi)$ is the (log) base measure.

Now we rewrite $A(\vec{\eta}_d(\vec{z}; \Theta))$ in terms of the entropy of $p_{\Theta}(x_d | \vec{z})$ and other terms. For this we use the definition of the entropy and obtain using the parametrization with natural parameters:

$$\begin{aligned} \mathcal{H}[p_{\Theta}(x_d | \vec{z})] &= - \int p_{\Theta}(x_d | \vec{z}) \log(p_{\Theta}(x_d | \vec{z})) dx_d \\ &= - \int p_{\Theta}(x_d | \vec{z}) \left(-\frac{1}{2} \log(2\pi) + \vec{\eta}_d^{\top}(\vec{z}; \Theta) \vec{T}(x_d^{(n)}) - A(\vec{\eta}_d(\vec{z}; \Theta)) \right) dx_d \\ &= - \vec{\eta}_d^{\top}(\vec{z}; \Theta) \mathbb{E}_{p_{\Theta}(x_d | \vec{z})} \{ \vec{T}(x_d^{(n)}) \} + A(\vec{\eta}_d(\vec{z}; \Theta)) + \frac{1}{2} \log(2\pi) \\ &= - \vec{\eta}_d^{\top}(\vec{z}; \Theta) \frac{d}{d\vec{\eta}} A(\vec{\eta}) \Big|_{\vec{\eta}=\vec{\eta}_d(\vec{z}; \Theta)} + A(\vec{\eta}_d(\vec{z}; \Theta)) + \frac{1}{2} \log(2\pi) \end{aligned} \quad (46)$$

where we have used the standard equality $\mathbb{E}_{p(x|\vec{\eta})} \{ \vec{T}(x) \} = \frac{d}{d\vec{\eta}} A(\vec{\eta})$ which applies for the Gaussian as exponential family distribution. We further abbreviate using $\vec{A}' = \frac{d}{d\vec{\eta}} A(\vec{\eta})$ and obtain:

$$-A(\vec{\eta}_d(\vec{z}; \Theta)) - \frac{1}{2} \log(2\pi) = - \vec{\eta}_d^{\top}(\vec{z}; \Theta) \vec{A}'(\vec{\eta}_d(\vec{z}; \Theta)) - \mathcal{H}[p_{\Theta}(x_d | \vec{z})]$$

By inserting this expression into (43) we can consequently express $\mathcal{F}_2(\Phi, \Theta)$ as follows:

$$\mathcal{F}_2(\Phi, \Theta) = \frac{1}{N} \sum_{n=1}^N \sum_{d=1}^D \int q_{\Phi}^{(n)}(\vec{z}) \left(\vec{\eta}_d^{\top}(\vec{z}; \Theta) \vec{T}(x_d^{(n)}) - \vec{\eta}_d^{\top}(\vec{z}; \Theta) \vec{A}'(\vec{\eta}_d(\vec{z}; \Theta)) - \mathcal{H}[p_{\Theta}(x_d | \vec{z})] \right) d\vec{z} \quad (47)$$

Expression (47) is the generalization of (15) for general $\sigma_d^2(\vec{z}; \Theta)$. As for the proof of Prop. 1, we now seek to show that all terms of (47) except the one depending on $\mathcal{H}[p_{\Theta}(x_d | \vec{z})]$ are zero at stationary points.

Let us first abbreviate the networks DNN_{μ} and DNN_{σ} of the decoder (Eqn. 30) as follows:

$$\mu_d(\vec{z}; \Theta) = (\text{DNN}_{\mu}(\vec{z}; W))_d = \sum_i W_{di}^{(L)} \varphi_i^{\mu}(\vec{z}; \Theta) \quad (48)$$

$$\sigma_d^2(\vec{z}; \Theta) = (\text{DNN}_{\sigma}(\vec{z}; M))_d = \sum_j M_{dj}^{(L)} \varphi_j^{\sigma}(\vec{z}; \Theta), \quad (49)$$

where $\varphi_i^{\mu}(\vec{z}; \Theta)$ and $\varphi_j^{\sigma}(\vec{z}; \Theta)$ simply stand for the remainder of the DNN after the lowest weights are removed. We demanded that the decoder networks both have at least one hidden layer such that $L \geq 1$, i.e., the weights $W^{(L)}$ and $M^{(L)}$ are different from the weight matrices $W^{(0)}$ and $M^{(0)}$. Hence, we do not have to worry about any constraints that are potentially introduced for $W^{(0)}$ and $M^{(0)}$. At all stationary points of the variational lower bound $\mathcal{F}(\Phi, \Theta)$ it thus applies:

$$\frac{d}{dW^{(L)}} \mathcal{F}(\Phi, \Theta) = \frac{d}{dW^{(L)}} \mathcal{F}_2(\Phi, \Theta) = 0, \quad \text{and} \quad \frac{d}{dM^{(L)}} \mathcal{F}(\Phi, \Theta) = \frac{d}{dM^{(L)}} \mathcal{F}_2(\Phi, \Theta) = 0. \quad (50)$$

The derivative w.r.t. $\mathcal{F}_2(\Phi, \Theta)$ is zero as the other terms of $\mathcal{F}(\Phi, \Theta)$ (i.e., $\mathcal{F}_1(\Phi, \Theta)$ and $\mathcal{F}_3(\Phi)$) do not depend on $W^{(L)}$ and $M^{(L)}$. Let us now arrange all entries of $W^{(L)}$ and $M^{(L)}$ into one long vector which we shall call \vec{R} . Let us denote by \vec{R}^* a fixed stationary point that we consider. All the following derivations can be considered to apply for one such stationary point \vec{R}^* . But as any stationary point \vec{R}^* can be considered, all the following derivations will apply for all possible stationary points \vec{R}^* .

Let us now borrow methodology from variational calculus, i.e., we use that for arbitrary parameters \vec{R} the following applies at the stationary points \vec{R}^* :

$$\left. \frac{d}{d\epsilon} \mathcal{F}_2(\Phi, \vec{R}^* + \epsilon \vec{R}) \right|_{\epsilon=0} = 0, \quad (51)$$

where we neglected all parameters Θ other than W and M in the argument of \mathcal{F}_2 for readability. We will also do so in the following, and furthermore will write $p(x_d | \vec{z}; \vec{R})$ instead of $p_\Theta(x_d | \vec{z})$.

Eqn. (51) combines the above conditions (50), and we can proceed by taking derivatives w.r.t. the scalar ϵ . Inserting the expression (47) for \mathcal{F}_2 into (51), we obtain:

$$\begin{aligned} & \frac{d}{d\epsilon} \mathcal{F}_2(\Phi, \vec{R}^* + \epsilon \vec{R}) \\ &= \frac{1}{N} \sum_{n,d} \int q_\Phi^{(n)}(\vec{z}) \frac{d}{d\epsilon} \left[\vec{\eta}_d^\top(\vec{z}; \vec{R}^* + \epsilon \vec{R}) \vec{T}(x_d^{(n)}) - \vec{\eta}_d^\top(\vec{z}; \vec{R}^* + \epsilon \vec{R}) \vec{A}'(\vec{\eta}_d(\vec{z}; \vec{R}^* + \epsilon \vec{R})) \right. \\ & \quad \left. - \mathcal{H}[p(x_d | \vec{z}; \vec{R}^* + \epsilon \vec{R})] \right] d\vec{z} \\ &= \frac{1}{N} \sum_{n,d} \int q_\Phi^{(n)}(\vec{z}) \left[\left(\frac{d}{d\epsilon} \vec{\eta}_d^\top(\vec{z}; \vec{R}^* + \epsilon \vec{R}) \right) \vec{T}(x_d^{(n)}) - \left(\frac{d}{d\epsilon} \vec{\eta}_d^\top(\vec{z}; \vec{R}^* + \epsilon \vec{R}) \right) \vec{A}'(\vec{\eta}_d(\vec{z}; \vec{R}^* + \epsilon \vec{R})) \right. \\ & \quad \left. - \vec{\eta}_d^\top(\vec{z}; \vec{R}^* + \epsilon \vec{R}) \left(\frac{d}{d\epsilon} \vec{A}'(\vec{\eta}_d(\vec{z}; \vec{R}^* + \epsilon \vec{R})) \right) - \frac{d}{d\epsilon} \mathcal{H}[p(x_d | \vec{z}; \vec{R}^* + \epsilon \vec{R})] \right] d\vec{z}. \end{aligned} \quad (52)$$

The derivative of the entropy can now be determined using the expression (46) that we already used above:

$$\begin{aligned} & \frac{d}{d\epsilon} \mathcal{H}[p(x_d | \vec{z}; \vec{R}^* + \epsilon \vec{R})] \\ &= - \frac{d}{d\epsilon} \left(\vec{\eta}_d^\top(\vec{z}; \vec{R}^* + \epsilon \vec{R}) \vec{A}'(\vec{\eta}_d(\vec{z}; \vec{R}^* + \epsilon \vec{R})) \right) + \frac{d}{d\epsilon} A(\vec{\eta}_d(\vec{z}; \vec{R}^* + \epsilon \vec{R})) \\ &= - \left(\frac{d}{d\epsilon} \vec{\eta}_d^\top(\vec{z}; \vec{R}^* + \epsilon \vec{R}) \right) \vec{A}'(\vec{\eta}_d(\vec{z}; \vec{R}^* + \epsilon \vec{R})) \\ & \quad - \vec{\eta}_d^\top(\vec{z}; \vec{R}^* + \epsilon \vec{R}) \frac{d}{d\epsilon} \vec{A}'(\vec{\eta}_d(\vec{z}; \vec{R}^* + \epsilon \vec{R})) + \frac{d}{d\epsilon} A(\vec{\eta}_d(\vec{z}; \vec{R}^* + \epsilon \vec{R})). \end{aligned} \quad (53)$$

By inserting this expression back into (52), the two first terms (importantly) cancel with two terms of (52) and we obtain:

$$\begin{aligned} & \frac{d}{d\epsilon} \mathcal{F}_2(\Phi, \vec{R}^* + \epsilon \vec{R}) \\ &= \frac{1}{N} \sum_{n,d} \int q_\Phi^{(n)}(\vec{z}) \left[\left(\frac{d}{d\epsilon} \vec{\eta}_d^\top(\vec{z}; \vec{R}^* + \epsilon \vec{R}) \right) \vec{T}(x_d^{(n)}) - \frac{d}{d\epsilon} A(\vec{\eta}_d(\vec{z}; \vec{R}^* + \epsilon \vec{R})) \right] d\vec{z} \\ &= \frac{1}{N} \sum_{n,d} \int q_\Phi^{(n)}(\vec{z}) \left[\left(\frac{d}{d\epsilon} \vec{\eta}_d^\top(\vec{z}; \vec{R}^* + \epsilon \vec{R}) \right) \vec{T}(x_d^{(n)}) - \left(\frac{d}{d\epsilon} \vec{\eta}_d^\top(\vec{z}; \vec{R}^* + \epsilon \vec{R}) \right) \vec{A}'(\vec{\eta}_d(\vec{z}; \vec{R}^* + \epsilon \vec{R})) \right] d\vec{z} \\ &= \frac{1}{N} \sum_{n,d} \int q_\Phi^{(n)}(\vec{z}) \left(\frac{d}{d\epsilon} \vec{\eta}_d^\top(\vec{z}; \vec{R}^* + \epsilon \vec{R}) \right) \left[\vec{T}(x_d^{(n)}) - \vec{A}'(\vec{\eta}_d(\vec{z}; \vec{R}^* + \epsilon \vec{R})) \right] d\vec{z} \end{aligned}$$

The derivative w.r.t. ϵ is in the above expression now restricted to $\vec{\eta}_d$. If we evaluate at stationary points, i.e. for $\epsilon = 0$, we obtain:

$$\begin{aligned} 0 &= \left. \frac{d}{d\epsilon} \mathcal{F}_2(\Phi, \vec{R}^* + \epsilon \vec{R}) \right|_{\epsilon=0} \\ &= \frac{1}{N} \sum_{n,d} \int q_\Phi^{(n)}(\vec{z}) \left(\left. \frac{d}{d\epsilon} \vec{\eta}_d^\top(\vec{z}; \vec{R}^* + \epsilon \vec{R}) \right|_{\epsilon=0} \right) \left[\vec{T}(x_d^{(n)}) - \vec{A}'(\vec{\eta}_d(\vec{z}; \vec{R}^*)) \right] d\vec{z}. \end{aligned} \quad (54)$$

Expression (54) can be compared with expression (47) which expresses the lower bound (for any parameters) in terms of the entropy. The part of (47) which is not depending on the entropy is given by

$$\frac{1}{N} \sum_{n=1}^N \sum_{d=1}^D \int q_{\Phi}^{(n)}(\vec{z}) \vec{\eta}_d^T(\vec{z}; \vec{R}) \left[\vec{T}(x_d^{(n)}) - \vec{A}'(\vec{\eta}_d(\vec{z}; \vec{R})) \right] d\vec{z}. \quad (55)$$

If we can show that (55) is zero at stationary points \vec{R}^* , then we have proven that \mathcal{F}_2 converges to an expected entropy (as desired). However, we can not directly conclude from (54) that (55) is zero – the middle factors of the integrands differ. On the other hand, (54) applies for any vector \vec{R} . In the following, we will therefore try to choose \vec{R} in a way that allows to conclude that (55) is zero. As preparation, let us reformulate (54) as follows:

$$\begin{aligned} 0 &= \frac{d}{d\epsilon} \mathcal{F}_2(\Phi, \vec{R}^* + \epsilon \vec{R})|_{\epsilon=0} \\ &= \frac{1}{N} \sum_{n,d} \int q_{\Phi}^{(n)}(\vec{z}) \left(\frac{d}{d\epsilon} \vec{\eta}_d^T(\vec{z}; \vec{R}^* + \epsilon \vec{R})|_{\epsilon=0} \right) \left[\vec{T}(x_d^{(n)}) - \vec{A}'(\vec{\eta}_d(\vec{z}; \vec{R}^*)) \right] d\vec{z} \\ &= \frac{1}{N} \sum_{n,d} \int q_{\Phi}^{(n)}(\vec{z}) \left(\begin{array}{c} \left(\frac{d}{d\vec{R}} \eta_d^{(1)}(\vec{z}; \vec{R})|_{\vec{R}=\vec{R}^*} \right) \vec{R} \\ \left(\frac{d}{d\vec{R}} \eta_d^{(2)}(\vec{z}; \vec{R})|_{\vec{R}=\vec{R}^*} \right) \vec{R} \end{array} \right)^T \left[\vec{T}(x_d^{(n)}) - \vec{A}'(\vec{\eta}_d(\vec{z}; \vec{R}^*)) \right] d\vec{z} \\ &= \frac{1}{N} \sum_{n,d} \int q_{\Phi}^{(n)}(\vec{z}) \left(\frac{d}{d\vec{R}} \eta_d^{(1)}(\vec{z}; \vec{R})|_{\vec{R}=\vec{R}^*} \right) \vec{R} \left(T^{(1)}(x_d^{(n)}) - \frac{d}{d\eta^{(1)}} A(\vec{\eta})|_{\vec{\eta}=\vec{\eta}_d(\vec{z}; \vec{R}^*)} \right) d\vec{z} \\ &\quad + \frac{1}{N} \sum_{n,d} \int q_{\Phi}^{(n)}(\vec{z}) \left(\frac{d}{d\vec{R}} \eta_d^{(2)}(\vec{z}; \vec{R})|_{\vec{R}=\vec{R}^*} \right) \vec{R} \left(T^{(2)}(x_d^{(n)}) - \frac{d}{d\eta^{(2)}} A(\vec{\eta})|_{\vec{\eta}=\vec{\eta}_d(\vec{z}; \vec{R}^*)} \right) d\vec{z} \end{aligned} \quad (56)$$

We now defined the vector \vec{R} to contain all elements of W and M in one (long) row vector. To further evaluate (56), we have to evaluate the derivatives of $\eta_d^{(1)}(\vec{z}; \vec{R})$ and $\eta_d^{(2)}(\vec{z}; \vec{R})$ w.r.t. all the entries. Eqn. (44) describes the relation between the natural parameters $\eta_d^{(1)}(\vec{z}; \vec{R})$ and $\eta_d^{(2)}(\vec{z}; \vec{R})$ and the decoder DNNs $\mu_d(\vec{z}; \vec{R})$ and $\sigma_d^2(\vec{z}; \vec{R})$. If we use for the DNNs abbreviations (48) and (49), we can evaluate the derivatives. We demanded two separate sets of parameters for the DNNs, i.e., $\mu_d(\vec{z}; \vec{R})$ only depends on W and $\sigma_d^2(\vec{z}; \vec{R})$ only depends on M . We therefore obtain:

$$\begin{aligned} &\frac{d}{dW_{di}^{(L)}} \eta_{d'}^{(1)}(\vec{z}; \vec{R}) && \frac{d}{dM_{dj}^{(L)}} \eta_{d'}^{(1)}(\vec{z}; \vec{R}) \\ &= \frac{1}{\sigma_{d'}^2(\vec{z}; \vec{R})} \frac{d}{dW_{di}^{(L)}} \mu_{d'}(\vec{z}; \vec{R}) && = \mu_d(\vec{z}; \vec{R}) \frac{d}{dM_{dj}^{(L)}} \frac{1}{\sigma_{d'}^2(\vec{z}; \vec{R})} \\ &= \frac{1}{\sigma_{d'}^2(\vec{z}; \vec{R})} \frac{d}{dW_{di}^{(L)}} \sum_{i'} W_{d'i'}^{(L)} \varphi_{i'}^{\mu}(\vec{z}; \vec{R}) && = -\frac{\mu_d(\vec{z}; \vec{R})}{\sigma_{d'}^4(\vec{z}; \vec{R})} \frac{d}{dM_{dj}^{(L)}} \sum_{j'} M_{d'j'}^{(L)} \varphi_{j'}^{\sigma}(\vec{z}; \vec{R}) \\ &= \delta_{dd'} \frac{1}{\sigma_d^2(\vec{z}; \vec{R})} \varphi_i^{\mu}(\vec{z}; \vec{R}), && = -\delta_{dd'} \frac{\mu_d(\vec{z}; \vec{R})}{\sigma_d^4(\vec{z}; \vec{R})} \varphi_j^{\sigma}(\vec{z}; \vec{R}), \\ \\ &\frac{d}{dW_{di}^{(L)}} \eta_{d'}^{(2)}(\vec{z}; \vec{R}) && \frac{d}{dM_{dj}^{(L)}} \eta_{d'}^{(2)}(\vec{z}; \vec{R}) \\ &= -\frac{1}{2} \frac{d}{dW_{di}^{(L)}} \frac{1}{\sigma_{d'}^2(\vec{z}; \vec{R})} && = -\frac{1}{2} \frac{d}{dM_{dj}^{(L)}} \frac{1}{\sigma_{d'}^2(\vec{z}; \vec{R})} \\ &= 0 && = \frac{1}{2} \frac{1}{\sigma_{d'}^4(\vec{z}; \vec{R})} \frac{d}{dM_{dj}^{(L)}} \sum_{j'} M_{d'j'}^{(L)} \varphi_{j'}^{\sigma}(\vec{z}; \vec{R}) \\ &&& = \frac{1}{2} \delta_{dd'} \frac{1}{\sigma_d^4(\vec{z}; \vec{R})} \varphi_j^{\sigma}(\vec{z}; \vec{R}) \end{aligned}$$

Using these expressions, we can (considering Eqn. 56) evaluate the terms

$$\left(\frac{d}{d\vec{R}} \eta_d^{(1)}(\vec{z}; \vec{R})|_{\vec{R}=\vec{R}^*} \right) \vec{R} \quad \text{and} \quad \left(\frac{d}{d\vec{R}} \eta_d^{(2)}(\vec{z}; \vec{R})|_{\vec{R}=\vec{R}^*} \right) \vec{R} \quad (57)$$

for specifically chosen $\tilde{\vec{R}}$ (keep in mind that Eqn. 56 holds for any $\tilde{\vec{R}}$). Let us choose $\tilde{\vec{R}}$ to be zero almost everywhere, only those entries for $W_{di}^{(L)}$ we keep non-zero. We then obtain:

$$\left(\frac{d}{d\tilde{\vec{R}}}\eta_{a'}^{(1)}(\vec{z}; \tilde{\vec{R}})|_{\tilde{\vec{R}}=\tilde{\vec{R}}^*}\right)\tilde{\vec{R}} = \sum_d \sum_i \left(\frac{d}{dW_{di}^{(L)}}\eta_{a'}^{(1)}(\vec{z}; \tilde{\vec{R}})\right)|_{\tilde{\vec{R}}=\tilde{\vec{R}}^*} W_{di}^{(L)} \quad (58)$$

$$= \sum_d \sum_i \left(\delta_{da'} \frac{1}{\sigma_d^2(\vec{z}; \tilde{\vec{R}}^*)} \varphi_i^\mu(\vec{z}; \tilde{\vec{R}}^*)\right) W_{di}^{(L)} = \frac{1}{\sigma_{a'}^2(\vec{z}; \tilde{\vec{R}}^*)} \sum_i W_{a'i}^{(L)} \varphi_i^\mu(\vec{z}; \tilde{\vec{R}}^*) \quad (59)$$

$$= \frac{1}{\sigma_{a'}^2(\vec{z}; \tilde{\vec{R}}^*)} \mu_{a'}(\vec{z}; \tilde{\vec{R}}^*) = \eta_{a'}^{(1)}(\vec{z}; \tilde{\vec{R}}^*), \quad \text{and further} \quad (60)$$

$$\left(\frac{d}{d\tilde{\vec{R}}}\eta_{a'}^{(2)}(\vec{z}; \tilde{\vec{R}})|_{\tilde{\vec{R}}=\tilde{\vec{R}}^*}\right)\tilde{\vec{R}} = \sum_d \sum_i \left(\frac{d}{dW_{di}^{(L)}}\eta_{a'}^{(2)}(\vec{z}; \tilde{\vec{R}})\right)|_{\tilde{\vec{R}}=\tilde{\vec{R}}^*} W_{di}^{(L)} = 0, \quad (61)$$

where for the line (59) we have chosen $W_{di}^{(L)}$ not to be arbitrary non-zero entries of $\tilde{\vec{R}}$ but those at the stationary points (we are free to choose any value). The reason why we can relate the derivative of $\eta_{a'}^{(1)}$ to $\eta_{a'}^{(1)}$ itself is that the lowest stage of both DNNs is a linear operation. Consequently, the relation can not necessarily be derived for general functions $\mu_a(\vec{z}; \tilde{\vec{R}})$ and $\sigma_d^2(\vec{z}; \tilde{\vec{R}})$ but it can be fulfilled for the standard DNNs we consider. By inserting (60) and (61) into (56) we obtain that at stationary points $\tilde{\vec{R}}^*$ holds:

$$\begin{aligned} 0 &= \frac{d}{d\epsilon} \mathcal{F}_2(\Phi, \tilde{\vec{R}}^* + \epsilon \tilde{\vec{R}})|_{\epsilon=0} \\ &= \frac{1}{N} \sum_{n,d} \int q_\Phi^{(n)}(\vec{z}) \eta_d^{(1)}(\vec{z}; \tilde{\vec{R}}^*) \left(T^{(1)}(x_d^{(n)}) - \frac{d}{d\eta^{(1)}} A(\vec{\eta})|_{\vec{\eta}=\vec{\eta}_d(\vec{z}; \tilde{\vec{R}}^*)}\right) d\vec{z} \end{aligned} \quad (62)$$

By comparing with (55) we observe that the first summand of the integrand is zero at $\tilde{\vec{R}}^*$. However, we also have to show that the second summand (with $\eta_d^{(2)}(\vec{z}; \tilde{\vec{R}}^*)$) is zero. We still have the liberty to choose other $\tilde{\vec{R}}$ for (56). A complementary choice to the $\tilde{\vec{R}}$ chosen above would be to choose all entries of $\tilde{\vec{R}}$ to be zero except of those corresponding to the entries of $M_{dj}^{(L)}$. If we do so, we obtain:

$$\left(\frac{d}{d\tilde{\vec{R}}}\eta_{a'}^{(1)}(\vec{z}; \tilde{\vec{R}})|_{\tilde{\vec{R}}=\tilde{\vec{R}}^*}\right)\tilde{\vec{R}} = \sum_d \sum_j \left(\frac{d}{dM_{dj}^{(L)}}\eta_{a'}^{(1)}(\vec{z}; \tilde{\vec{R}})\right)|_{\tilde{\vec{R}}=\tilde{\vec{R}}^*} M_{dj}^{(L)} \quad (63)$$

$$= \sum_d \sum_j \left(-\delta_{da'} \frac{\mu_d(\vec{z}; \tilde{\vec{R}})}{\sigma_d^4(\vec{z}; \tilde{\vec{R}})} \varphi_j^\sigma(\vec{z}; \tilde{\vec{R}})\right) M_{dj}^{(L)} = -\frac{\mu_{a'}(\vec{z}; \tilde{\vec{R}})}{\sigma_{a'}^4(\vec{z}; \tilde{\vec{R}})} \sum_j M_{a'j}^{(L)} \varphi_j^\sigma(\vec{z}; \tilde{\vec{R}}) \quad (64)$$

$$= -\frac{\mu_{a'}(\vec{z}; \tilde{\vec{R}})}{\sigma_{a'}^4(\vec{z}; \tilde{\vec{R}})} \sigma_{a'}^2(\vec{z}; \tilde{\vec{R}}) = -\frac{\mu_{a'}(\vec{z}; \tilde{\vec{R}})}{\sigma_{a'}^2(\vec{z}; \tilde{\vec{R}})} = -\eta_{a'}^{(1)}(\vec{z}; \tilde{\vec{R}}^*), \quad \text{and further} \quad (65)$$

$$\left(\frac{d}{d\tilde{\vec{R}}}\eta_{a'}^{(2)}(\vec{z}; \tilde{\vec{R}})|_{\tilde{\vec{R}}=\tilde{\vec{R}}^*}\right)\tilde{\vec{R}} = \sum_d \sum_j \left(\frac{d}{dM_{dj}^{(L)}}\eta_{a'}^{(2)}(\vec{z}; \tilde{\vec{R}})\right)|_{\tilde{\vec{R}}=\tilde{\vec{R}}^*} M_{dj}^{(L)} \quad (66)$$

$$= \sum_d \sum_j \left(\frac{1}{2} \delta_{da'} \frac{1}{\sigma_d^4(\vec{z}; \tilde{\vec{R}}^*)} \varphi_j^\sigma(\vec{z}; \tilde{\vec{R}}^*)\right) M_{dj}^{(L)} = \frac{1}{2} \frac{1}{\sigma_{a'}^4(\vec{z}; \tilde{\vec{R}}^*)} \sum_j M_{a'j}^{(L)} \varphi_j^\sigma(\vec{z}; \tilde{\vec{R}}^*) \quad (67)$$

$$= \frac{1}{2} \frac{1}{\sigma_{a'}^4(\vec{z}; \tilde{\vec{R}}^*)} \sigma_{a'}^2(\vec{z}; \tilde{\vec{R}}^*) = \frac{1}{2} \frac{1}{\sigma_{a'}^2(\vec{z}; \tilde{\vec{R}}^*)} = -\eta_{a'}^{(2)}(\vec{z}; \tilde{\vec{R}}^*) \quad (68)$$

By inserting (65) and (68) into (56) we obtain:

$$\begin{aligned}
0 &= \frac{d}{d\epsilon} \mathcal{F}_2(\Phi, \vec{R}^* + \epsilon \tilde{\vec{R}})|_{\epsilon=0} \\
&= \frac{1}{N} \sum_{n,d} \int q_{\Phi}^{(n)}(\vec{z}) \left(\frac{d}{d\vec{R}} \eta_d^{(1)}(\vec{z}; \vec{R})|_{\vec{R}=\vec{R}^*} \right) \tilde{\vec{R}} \left(T^{(1)}(x_d^{(n)}) - \frac{d}{d\eta^{(1)}} \vec{A}(\vec{\eta})|_{\vec{\eta}=\vec{\eta}_d(\vec{z}; \vec{R}^*)} \right) d\vec{z} \\
&\quad + \frac{1}{N} \sum_{n,d} \int q_{\Phi}^{(n)}(\vec{z}) \left(\frac{d}{d\vec{R}} \eta_d^{(2)}(\vec{z}; \vec{R})|_{\vec{R}=\vec{R}^*} \right) \tilde{\vec{R}} \left(T^{(2)}(x_d^{(n)}) - \frac{d}{d\eta^{(2)}} \vec{A}(\vec{\eta})|_{\vec{\eta}=\vec{\eta}_d(\vec{z}; \vec{R}^*)} \right) d\vec{z} \tag{69}
\end{aligned}$$

$$\begin{aligned}
&= \frac{1}{N} \sum_{n,d} \int q_{\Phi}^{(n)}(\vec{z}) \left(-\eta_d^{(1)}(\vec{z}; \vec{R}^*) \right) \left(T^{(1)}(x_d^{(n)}) - \frac{d}{d\eta^{(1)}} \vec{A}(\vec{\eta})|_{\vec{\eta}=\vec{\eta}_d(\vec{z}; \vec{R}^*)} \right) d\vec{z} \\
&\quad + \frac{1}{N} \sum_{n,d} \int q_{\Phi}^{(n)}(\vec{z}) \left(-\eta_d^{(2)}(\vec{z}; \vec{R}^*) \right) \left(T^{(2)}(x_d^{(n)}) - \frac{d}{d\eta^{(2)}} \vec{A}(\vec{\eta})|_{\vec{\eta}=\vec{\eta}_d(\vec{z}; \vec{R}^*)} \right) d\vec{z} \tag{70}
\end{aligned}$$

We have already shown above (62) that the first term with $\eta_d^{(1)}(\vec{z}; \vec{R}^*)$ is zero, which means that we can conclude:

$$0 = \frac{1}{N} \sum_{n,d} \int q_{\Phi}^{(n)}(\vec{z}) \eta_d^{(2)}(\vec{z}; \vec{R}^*) \left(T^{(2)}(x_d^{(n)}) - \frac{d}{d\eta^{(2)}} \vec{A}(\vec{\eta})|_{\vec{\eta}=\vec{\eta}_d(\vec{z}; \vec{R}^*)} \right) d\vec{z}. \tag{71}$$

Taking the intermediate results (62) and (71) together, we have shown that both summands that make up (55) are zero, i.e., expression (55) is zero at stationary point \vec{R}^* .

Therefore, we can finally go back to (47) and obtain at stationary point Θ^* (we go back again to full parameters):

$$\begin{aligned}
&\mathcal{F}_2(\Phi, \Theta^*) \\
&= \frac{1}{N} \sum_{n=1}^N \sum_{d=1}^D \int q_{\Phi}^{(n)}(\vec{z}) \left(\vec{\eta}_d^{\Gamma}(\vec{z}; \Theta^*) \vec{T}(x_d^{(n)}) - \vec{\eta}_d^{\Gamma}(\vec{z}; \Theta^*) \vec{A}'(\vec{\eta}_d(\vec{z}; \Theta^*)) - \mathcal{H}[p_{\Theta^*}(x_d | \vec{z})] \right) d\vec{z} \\
&= \frac{1}{N} \sum_{n=1}^N \sum_{d=1}^D \int q_{\Phi}^{(n)}(\vec{z}) \vec{\eta}_d^{\Gamma}(\vec{z}; \Theta^*) \left(\vec{T}(x_d^{(n)}) - \vec{A}'(\vec{\eta}_d(\vec{z}; \Theta^*)) \right) d\vec{z} \\
&\quad - \frac{1}{N} \sum_{n=1}^N \sum_{d=1}^D \int q_{\Phi}^{(n)}(\vec{z}) \mathcal{H}[p_{\Theta^*}(x_d | \vec{z})] d\vec{z} \\
&= -\frac{1}{N} \sum_{n=1}^N \int q_{\Phi}^{(n)}(\vec{z}) \mathcal{H}[p_{\Theta^*}(\vec{x} | \vec{z})] d\vec{z} = -\frac{1}{N} \sum_{n=1}^N \mathbb{E}_{q_{\Phi}^{(n)}} \{ \mathcal{H}[p_{\Theta^*}(\vec{x} | \vec{z})] \}. \tag{72}
\end{aligned}$$

With (72) we have thus arrived at the generalization of the term $\mathcal{F}_2(\Phi, \Theta)$ for \vec{z} -dependent decoder variances. The derivation for the terms $\mathcal{F}_1(\Phi, \Theta)$ and $\mathcal{F}_3(\Phi)$ follow along the same lines as for the proofs of Props. 1 and 2 with no changes to the final results for $\mathcal{F}_1(\Phi, \Theta)$ and $\mathcal{F}_3(\Phi)$, which proves the claim of Prop. 3. \square

Appendix D: Details of Numerical Experiments

We here provide further details on the numerical experiments of Sec. 3.

D.1 Generation of Artificial Data Sets and Learning Visualizations

We generated the PCA data set according to the following generative model of probabilistic PCA:

$$p(\vec{z}) = \mathcal{N}(\vec{z}; \vec{0}, \mathbb{1}) \tag{73}$$

$$p(\vec{x} | \vec{z}) = \mathcal{N}(\vec{x}; W_{\text{gen.}} \vec{z} + \vec{\mu}_{\text{gen.}}; \sigma_{\text{gen.}}^2 \mathbb{1}). \tag{74}$$

The generative parameters $W_{\text{gen.}}$ and $\vec{\mu}_{\text{gen.}}$ were drawn randomly from uniform distributions between 0 and 1 in each dimension for each new run. $\sigma_{\text{gen.}}$ was always set to 0.1. We used $H = 2$ as latent dimension and $D = 10$ as output dimension and generated 10.000 new training and testing data points for each experiment.

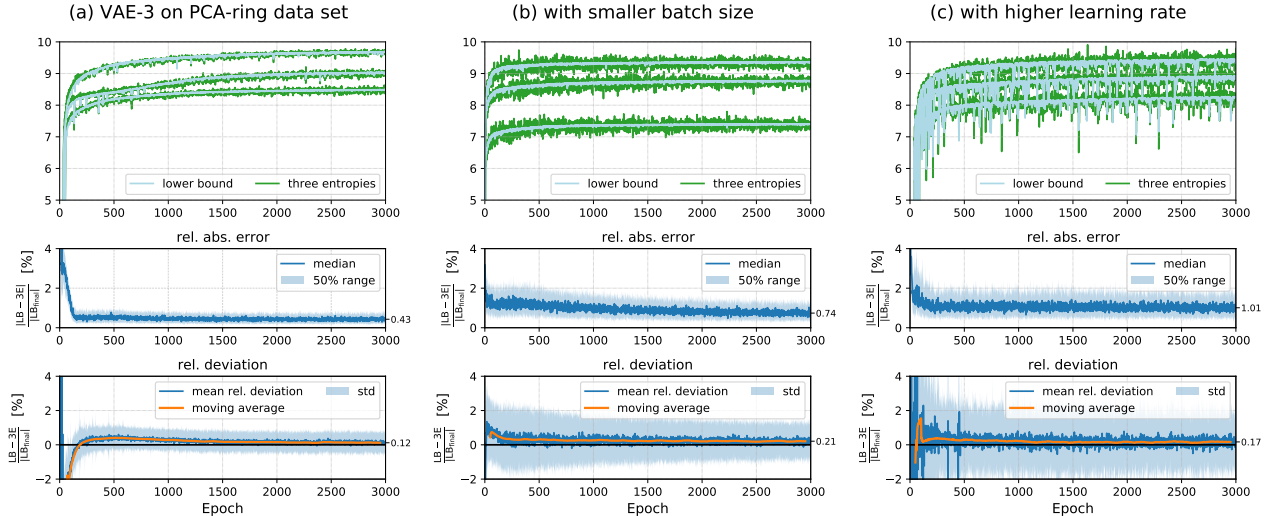


Figure 3: VAE-3 on PCA-ring data sets. The top two plots show experiments in the same way as Fig. 1: The top plot shows three independent runs on new randomly generated PCA-ring data each, while the middle plot shows the median of the relative absolute error between lower bound and three entropies over 100 such independent runs. Additionally we show the mean relative deviation (i.e., without taking absolute values) between lower bound and three entropies of these runs as bottom plots, together with the moving averages over 100 epochs. (a) shows experiment in the same setting as Fig. 1(c) over longer training time. (b) shows the same experiments with a batch size of 100 (compared to a batch size of 2000 in the other plots). (c) shows the same experiments with a learning rate of 0.005 (compared to a learning rate of 0.001 in the other plots).

For the PCA-ring data sets, we introduced an additional non-linear transformation $\vec{x}' = g(\vec{x})$ with

$$p(\vec{z}) = \mathcal{N}(\vec{z}; \vec{0}, \mathbb{1}) \quad (75)$$

$$p(\vec{x} | \vec{z}) = \mathcal{N}(\vec{x}; W_{\text{gen.}} \vec{z}; \sigma_{\text{gen.}}^2 \mathbb{1}) \quad (76)$$

$$\vec{x}' = \vec{\mu}_{\text{gen.}} + \frac{\vec{x}}{10} + \frac{\vec{x}}{|\vec{x}|} \quad (77)$$

projecting the data onto a ring-like structure in D -dimensional space (see, e.g., Doersch, 2016).

Fig. 4(c), on the last page, shows a PCA projection of the training data set, visualizations of the z - and x -space during training of VAE-3 as well as plots of the lower bound and the three entropies. Figs. 4(a) and (b) show the same plots for the linear VAE and VAE-1 on the PCA and MNIST data set, respectively. As expected, we see a slight overfitting of the linear VAE to the PCA training data, with the training log-likelihood converging to a value slightly above of the ground-truth. However, even with early stopping at around 700 iterations (see third segment of Fig. 4a), we see that the three entropies already compute the lower bound very well.

Animations that show different examples of the training process are available as part of the supplementary material.

D.2 Noise in Three Entropies and Lower Bound

The optimization of VAEs is stochastic due to finite learning rates, finite batch sizes and approximations of integrals over \vec{z} using sampling. A stationary point is consequently never fully converged to. Instead the parameters will finally stochastically fluctuate around a stationary point. In Fig. 1(c) we have (for VAE-3) numerically quantified the relative difference between the variational lower bound and Eqn. (31) of Prop. 3. As can be observed, and as stated in the main text, the values for the standard variational bound (5) and Eqn. (31) match very well in the region close to the stationary point (i.e. the region to which stochastic learning finally converges to). By evaluating over 100 runs, we observed an average *absolute* error of below 0.5% (i.e., 0.005) between the variational bound and Eqn. (31).

We can also further study the effect of stochasticity by using smaller batch sizes (Fig. 3b) or higher learning rates (Fig. 3c). In both cases, we obtain a higher stochasticity of the final fluctuations around the stationary

point. As a consequence, the average absolute error becomes larger (Fig. 3, middle row) but is still smaller-equal than 1% (i.e., 0.01). The change of the error with changing stochasticity is better observed for the absolute relative error than for the relative deviation (i.e., if we define the relative deviation as the relative absolute error but without taking magnitudes in the numerator, see Fig. 3, bottom row). However, for completeness, we also provide the relative deviation which is (as expected) smaller than the error (Fig. 3, bottom row). This means that the difference between variational lower bound and Eqn. (31) can be positive as well as negative close to the stationary point. Averaging cancels out the differences in large parts, which is the reason for the relative deviation being significantly smaller than the relative absolute error.

In summary, the numerical experiments provide (A) consistency with the theoretical result of Prop. 3 (and the other propositions), and (B) they show that the three entropies results of Props. 2 and 3 can provide very accurate estimations of the variational bound in practice. Note in this respect that the computation of final values of lower bounds always provides valuable information. Final lower bounds can be used as approximations to the true log-likelihood in many settings, and could be used for comparisons between different runs and/or different VAEs. Typical such comparisons can be applied for model selection, for instance. But also when the lower bounds are not good approximations of the log-likelihood, knowing their values at convergence is very useful to analyze learning: runs with high final values for variational lower bounds but low values for (held-out) log-likelihood indicate overfitting, for instance. The experiments of Figs. 1 and 3 show that the values of variational lower bounds can in practice easily be estimated with high accuracy. In the case of VAEs in the form of VAE-1, estimation with high accuracy is even possible using a closed-form expressions (see Prop. 2).

D.3 Implementation and Training Details

We used for all experiments a batch size of 2000, learning rates of $\epsilon = 10^{-3}$ and 100 samples (with the exception of Figs. 3b and 2c, as stated). These values were roughly chosen to give results with little fluctuations in the sampled lower bound and three entropies within reasonable time. The encoder and decoder DNNs for VAE-1 and VAE-3 were built with two hidden layers of 50 hidden units each and ReLU activations. Listing 1 shows an example PyTorch implementation of the linear VAE used in Fig. 1(a) as well as functions to compute the accumulated three entropies (i.e., summed over mini-batches) for the linear VAE, as well as VAE-1 and VAE-3.

Listing 1: Example Implementations

```

1 import torch
2 from torch.nn import Linear, Module, Parameter
3 from torch.nn.functional import softplus
4 from torch.distributions import Normal, kl_divergence
5 import math
6 pi = torch.Tensor([math.pi])
7
8 class LinearVAE(Module):
9     def __init__(self, H, D, num_samples=100):
10         super(LinearVAE, self).__init__()
11         self.H = H
12         self.D = D
13         self.num_samples = num_samples
14
15         self.encoder = Linear(D, H)
16         self.decoder = Linear(H, D)
17         self.noise_std = Parameter(torch.Tensor([0.]))
18         self.q_z_std = Parameter(torch.zeros(H))
19         self.p_z = Normal(torch.Tensor([0.]), torch.Tensor([1.]))
20
21     def forward(self, x):
22         sigma = softplus(self.noise_std)
23         tau = softplus(self.q_z_std)
24         N, D = x.shape
25
26         z_params = self.encoder(x)
27         q_z = Normal(z_params, tau)
28
29         z_samples = q_z.rsample([self.num_samples])
30         p_x_z_mean = self.decoder(z_samples)

```

```

31     p_x_z = Normal(p_x_z_mean, sigma)
32
33     lower_bound = p_x_z.log_prob(x).mean(0).sum() \
34                 - kl_divergence(q_z, self.p_z).sum()
35     three_entropies_linear = self.three_entropies_linear(N, D, sigma, tau)
36     return lower_bound, three_entropies_linear
37
38     @staticmethod
39     def three_entropies_linear(N, D, sigma, tau):
40         """Three Entropies (accumulated) for linear VAE, Eq.(33).
41         Args:
42             N (int) : batch size
43             D (int) : output dimensionality
44             sigma (torch.tensor, size=(1,)) : decoder standard deviation
45             tau (torch.tensor, size=(H,)) : encoder standard deviation
46         """
47         return N*(-D/2*(torch.log(2*pi)+1)-D*torch.log(sigma)+torch.log(tau).sum())
48
49     class VAE1(Module):
50
51         [...]
52
53         @staticmethod
54         def three_entropies_nonlinear(N, D, sigma, tau):
55             """Three Entropies (accumulated) for non-linear VAE (VAE-1), Eq.(25).
56             Args:
57                 N (int) : batch size
58                 D (int) : output dimensionality
59                 sigma (torch.tensor, size=(1,)) : decoder standard deviation
60                 tau (torch.tensor, size=(N, H)) : encoder standard deviation
61             """
62             return N*D*(-1/2*(torch.log(2*pi)+1)-torch.log(sigma)) + torch.log(tau).sum()
63
64     class VAE3(Module):
65
66         [...]
67
68         @staticmethod
69         def three_entropies_sigmaz(N, D, sigma, tau):
70             """Three Entropies (accumulated) for sigma(z)-VAE (VAE-3), Eq.(39).
71             Args:
72                 N (int) : batch size
73                 D (int) : output dimensionality
74                 sigma (torch.tensor, size=(num_samples, N, D)) : decoder std
75                 tau (torch.tensor, size=(N, H)) : encoder standard deviation
76             """
77             return -N*D/2*(torch.log(2*pi)+1) - torch.log(sigma).mean(0).sum() \
78                 + torch.log(tau).sum()

```

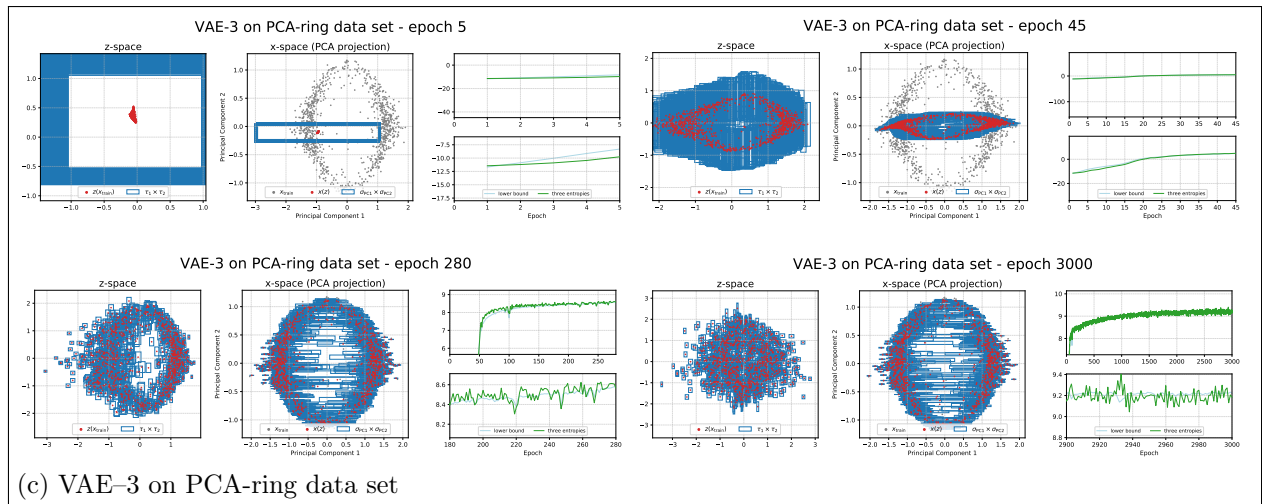
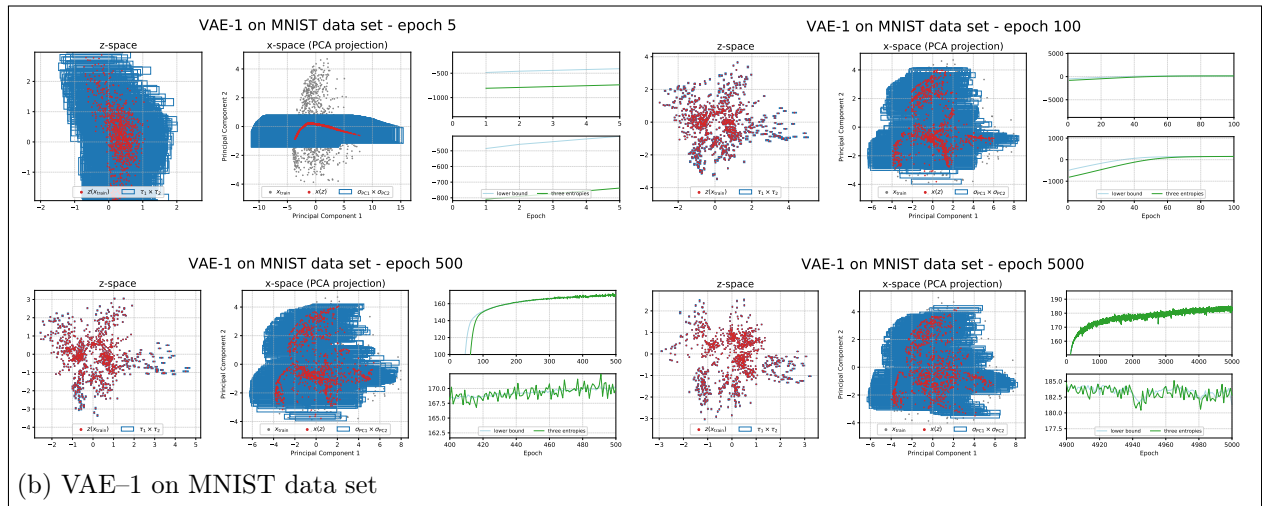
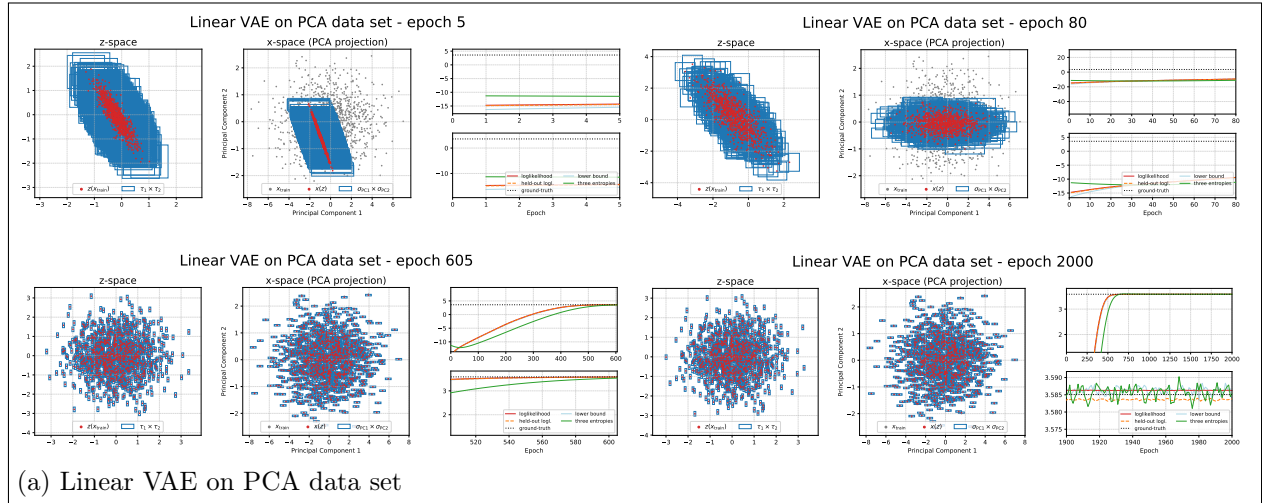



Figure 4: The training state of the VAEs of Fig. 1 is shown at four different points during training for each VAE on their respective data sets. The first plot of each segment shows 1000 \mathbf{z} -samples from the encoder in the 2-dimensional \mathbf{z} -space with the encoder standard deviation τ_h displayed as rectangle of width $2\tau_1$ and height $2\tau_2$. The second plot shows projections of the training data and of the 1000 $\hat{\mathbf{x}}(\mathbf{z})$ -reconstructions of the decoder to the first two PCA components of the training data, as well as the PCA projections of the decoder standard deviation as rectangle of width $2\sigma_{PC1}$ and height $2\sigma_{PC2}$. The last two plots show the sampled lower bound and the three entropies per data point, with the lower plots showing zoomed-in versions of the upper plots. For (a) the training, held-out and ground-truth log-likelihoods are shown additionally.